Keynote Lecture Series

Multi-modality imaging evaluation and pre-surgical planning for aortic valve-sparing operations in patients with aortic root aneurysm

Justin T. Tretter[1], Nelson H. Burbano-Vera[2], Hani K. Najm[1]

[1]Valve Procedural Planning Center, Department of Pediatric Cardiology and Division of Pediatric Cardiac Surgery, Cleveland Clinic Children's, and The Heart, Vascular, and Thoracic Institute, Cleveland Clinic, Cleveland, OH, USA; [2]Department of Cardiothoracic Anesthesiology, Anesthesiology Institute, Cleveland Clinic, Cleveland, OH, USA

Correspondence to: Justin T. Tretter, MD. Valve Procedural Planning Center, Department of Pediatric Cardiology and Division of Pediatric Cardiac Surgery, Cleveland Clinic Children's, and The Heart, Vascular, and Thoracic Institute, Cleveland Clinic, 9500 Euclid Avenue, M-41, Cleveland, OH 44195, USA. Email: trettej3@ccf.org.

Cardiac computed tomography (CT) and magnetic resonance (CMR) supplement echocardiography in the evaluation of those with aortic root and ascending aortic dilation, determining timing for intervention, guiding pre-surgical planning and post-operative surveillance. The dynamic, three-dimensional complexity of the aortic root and how it relates to the base of the left ventricle must be understood in any surgical approach addressing the aneurysmal aortic root. With improved imaging technology and the importance for proper patient counseling, it is no longer acceptable to enter the operating theater without a detailed blue print of what the problem is, and how best to address it. In addition, reliance on surgical expertise alone for intraoperative evaluation and decision making could be suboptimal due to the unloaded condition of the aortic root and the variance of experience of the surgeons to successfully repair the aortic valve. This is exemplified by the selective surgeons and centers who have the ability to tackle these aortic valve and root pathologies, compared to mitral valve repair techniques that have been codified and are generalizable. This review discusses a multimodality imaging approach in the patient with aortic root aneurysm, focusing on the precision added with pre-surgical CT assessment to guide aortic-valve sparing operations. This precision is afforded with a detailed understanding of the anatomy of the aortic root and underlying support, and its accurate evaluation by standard two- and three-dimensional imaging. Furthermore, we describe the evolving ability to predict the location of ventricular components of the atrioventricular conduction axis with further clinical imaging to personalize surgical strategies.

Keywords: Aortic root aneurysm; aortic valve surgery; computed tomography (CT); magnetic resonance; three-dimensional modeling

Submitted Mar 13, 2023. Accepted for publication May 30, 2023. Published online Jul 10, 2023.
doi: 10.21037/acs-2023-avs2-0040
View this article at: https://dx.doi.org/10.21037/acs-2023-avs2-0040

Introduction

Cardiac magnetic resonance (CMR) and computed tomography (CT) have well-established roles in monitoring those with aortic root and ascending aortic dilation, determining timing for intervention, guiding pre-surgical planning and post-operative surveillance. Both modalities play integral parts in the necessary multimodal imaging approach, with echocardiography serving as the mainstay of evaluation (1). Any surgical approach towards addressing the aneurysmal aortic root must appreciate the dynamic, three-dimensional (3D) complexity of both the normal aortic root, and that which is congenitally malformed (2,3). In addition, the surgeon must appreciate how the aortic root relates

to the base of the heart, including the predicted location of the ventricular components of the atrioventricular conduction axis (3). Historically, surgeons have largely depended on their intraoperative inspection to close the gap on decision making for surgical personalization. This is limited to a narrow field of view, time-pressure restrictions and evaluation in a non-hemodynamic state. This review discusses a multimodal imaging approach in the patient with aortic root aneurysm, focusing on the precision added with pre-surgical CT assessment to guide aortic valve-sparing operations. This precision can only be afforded with an understanding of the detailed anatomy of the aortic root and underlying support, and how accurately to assess this by standard two-dimensional (2D) and 3D imaging. Furthermore, we describe the evolving ability to predict the location of ventricular components of the atrioventricular conduction axis with clinical imaging further to personalize surgical strategies.

Evaluating the dilated aortic root: 3D understanding and imaging

It is without question that transthoracic echocardiography (TTE) remains the foothold in evaluation. Measurements of the proximal thoracic aorta, however, are often limited to 2D long axis assessment. This is where significant variability in the long axis plane may be introduced in assessing these dimensions (*Figure 1*) (4). Even with the ability for 3D echocardiographic imaging with multiplanar reformatting, there are variable differences in the axial and lateral spatial resolution that will be dictated by the best available acoustic window and any lung artifact (5). CMR or CT becomes necessary if any questions arise regarding accuracy in the assessment of aortic dimensions, and especially in those meeting criteria to proceed with intervention (6). Consistent high spatial resolution, cardiac gated 3D datasets are afforded by both CMR and CT. Additional respiratory gating is necessary in the former modality which necessitates longer acquisition times (3,7). CMR evaluation is often adequate as an adjunct to echocardiography for the serial follow-up of patients with aortic root and ascending aortic aneurysms who do not meet surgical thresholds (1,7). Furthermore, CMR may add value in the accurate assessment of significant aortic regurgitation, any corresponding left ventricular dilation and functional deterioration, and tissue characterization, with the avoidance of radiation exposure (8). Newer generation, dual source CT scanners have provided improved spatial and temporal resolution with significant decreases in radiation exposure, increasing the use of this modality in this patient population (9).

Virtual basal ring (echocardiographic annulus)

The virtual basal ring, or echocardiographic annulus, is a dynamic plane. Although often circular in systole, it becomes ovoid, elliptical or D-shaped in diastole when its valve aims to achieve competency (*Figures 2,3A,3B*) (3,4). Differences in this conformational change relates to the asymmetric support afforded by the base of the left ventricle to the aortic root. A portion of the left, and the entirety of the non-coronary sinuses are commonly supported by the fibrous tissue involving the aortic-mitral fibrous curtain, roof of the inferoseptal recess and membranous septum. It is the area supported by the aortic-mitral fibrous curtain that commonly can be found to be flattened, providing a D-shaped configuration during diastole. The muscular ventricular septum and free wall of the left ventricle then provide support to the entirety of the right, and portion of the left coronary sinuses (10). A variable degree of ventricular myocardium is incorporated into the bases of these coronary sinuses and under the base of the intervening interleaflet triangle, above the plane of the virtual basal ring (11). This feature then dictates the anatomical myocardial-arterial junction (*Figure 2*). Unlike the pulmonary root, this anatomical junction is found spanning between the coronary sinuses only (*Figure 2D*). Prior accounts simplifying this aortic junction to be completely annular, or equitable to the virtual basal ring, are incorrect. This understanding underlies the feasibility of the Ross procedure. The annular anatomical junction found within the pulmonary root allows it to be dissected out and used as an autograft. However, the lack of such an annular junction in the aortic root would not allow the same to be done with this arterial root (12). In the setting of aortic root dilation, its basal ring often is not spared. Its dilation may become asymmetric, leading to a less circular shape, even in systole (3).

Appreciating these intricacies, one can identify the clear pitfalls of any 2D long axis measurement of the virtual basal ring. If attempts are made to open up the widest dimensions between the right and non-coronary sinuses in long axis, this plane obtains at best an oblique cut across the virtual basal ring (*Figure 1*). Additionally, it remains challenging to ensure the nadirs of the two leaflets are being visualized, and that the basal ring plane is accurately identified. These shortcomings may add minimal inaccuracy if one aims

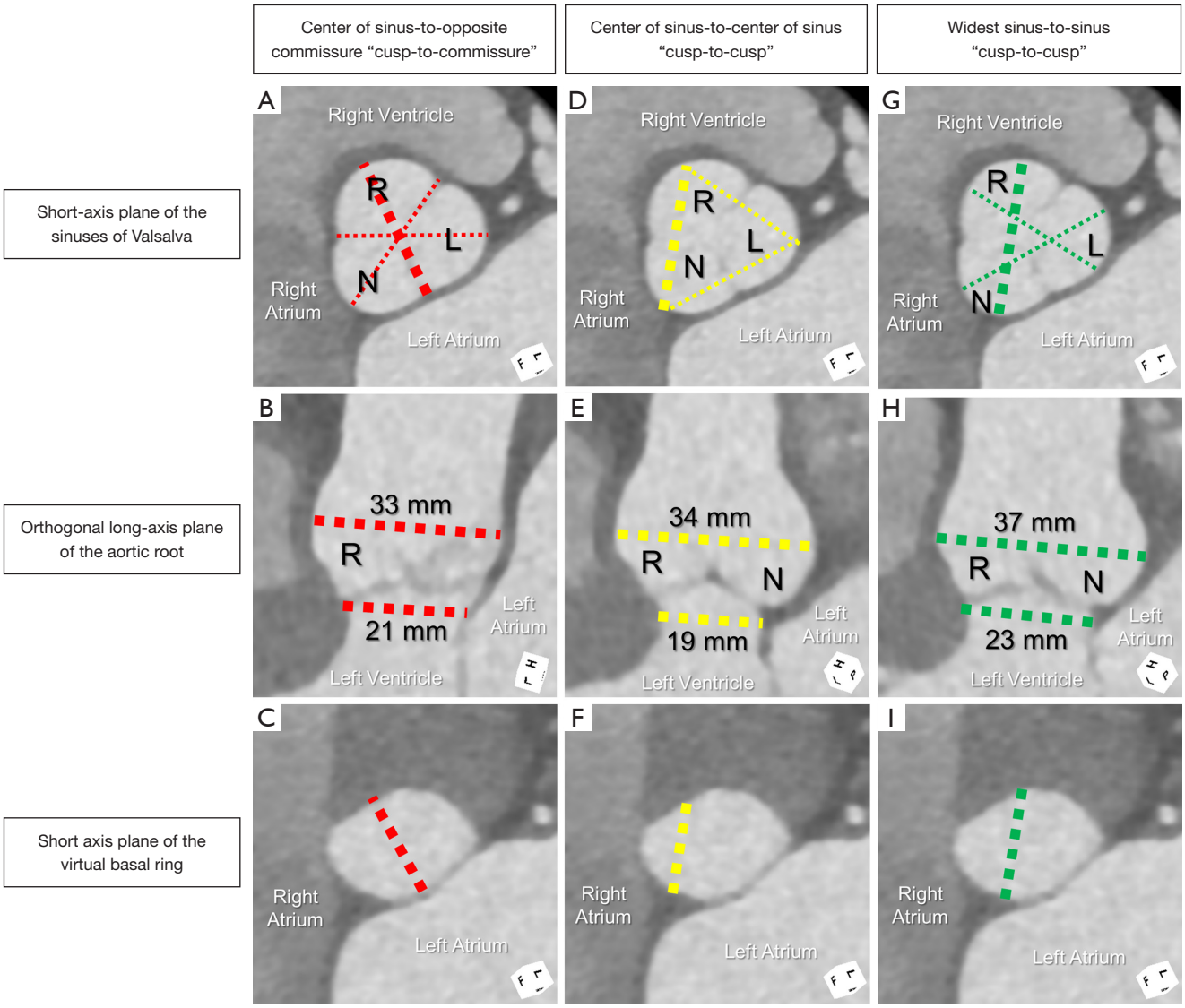

Figure 1 Comparison of 2D short- and long-axis assessment of the aortic root. The top row represents the three commonly used short axis measurements of the aortic root: center of sinus-to-opposite commissure (A), center of sinus-to-center of sinus (D), and widest sinus-to-sinus (G). The corresponding orthogonal long axis plane of the thicker dotted line is demonstrated in the middle row with the values listed for this specific patient (B,E,H). The relationship of how this plane cuts across the plane of the virtual basal ring is demonstrated in the lower row (C,F,I). This figure illustrates the variability in measurements of the aortic root and virtual basal ring obtained in 2D long-axis plane imaging and between the standard short axis measurements used in cross-sectional imaging. R, right coronary sinus; L, left coronary sinus; N, non-coronary sinus; 2D, two-dimensional.

solely to understand the systolic dimension, and despite dilation, the plane remains circular. For pre-surgical planning, however, if one aims to restore or maintain valve competency, understanding the diastolic dimensions becomes of equal importance. Such a measurement during diastole will represent an oblique measure of the minor axis of this plane, assuming this plane is accurately identified (*Figure 1C*,*1F*,*1I*).

Learning from the experience of transcatheter aortic valve replacement, we can add precision towards the assessment of the virtual basal ring utilizing cardiac gated cross-sectional 3D imaging. With multiplanar

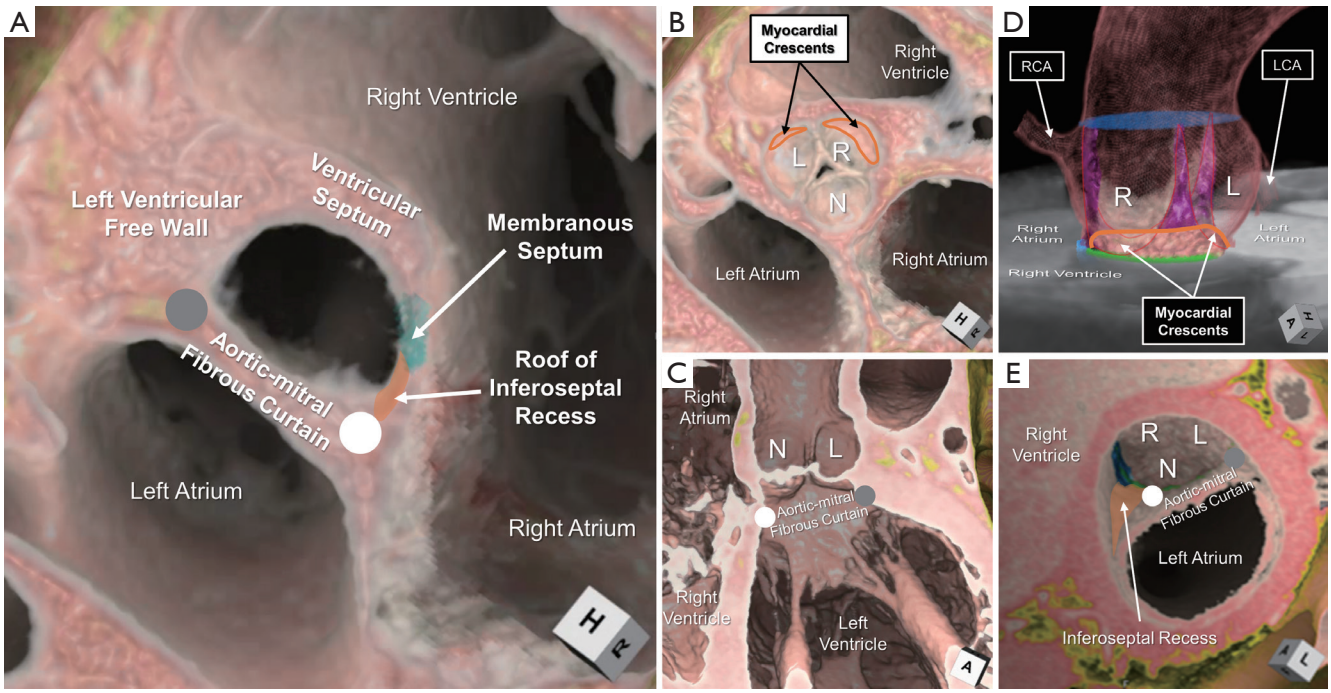

Figure 2 Anatomy of the aortic root and its underlying support. Using three-dimensional computed tomographic reconstructions, the ventricular support of the aortic root is demonstrated at the plane of the virtual basal ring (A), and compared to the sinuses of the aortic root (B). The right coronary sinus (R) and a portion of the left coronary sinus (L) are supported by the ventricular myocardium of the ventricular septum and left ventricular free wall. The non-coronary sinus (N) and portion of the left coronary sinus are supported by fibrous tissue. The fibrous tissue is comprised of the aortic-mitral fibrous curtain, spanned between the left (grey circle) and right fibrous trigones (white circle), and central fibrous body. The right fibrous trigone, roof of the inferoseptal recess (colored orange), and membranous septum (colored blue) form the central fibrous body. (C) The aortic-mitral fibrous curtain is the area of fibrous continuity between the anterior leaflet of the mitral valve and the aortic valve leaflets. (B,D) A variable amount of ventricular myocardium is incorporated into the bases of the coronary sinuses and at the base of their interposing interleaflet triangle (interleaflet triangles colored purple), above the plane of the virtual basal ring (colored green), forming the incomplete anatomical myocardial-arterial junction (orange line). The semilunar attachments of the leaflets (red lines) span between the virtual basal ring and sinutubular junction (colored blue). (E) Viewing from the apex of the left ventricle at the ventricular surface of the aortic valve leaflets, the central fibrous body is demonstrated to support a portion of the non-coronary sinuses and the base of the interleaflet triangle between the right and non-coronary sinuses. LCA, left coronary artery; RCA, right coronary artery.

reformatting, we can achieve the short axis of this plane, and precede with measurements. If the question is focused on valve preservation with root replacement in the incompetent valve, although systolic measures may be important, diastolic measurements will help compare to the measurements of the aortic valve discussed later. This helps to both understand the mechanism of incompetency, when present, and further to provide a quantitative road map on how to maintain or restore valve competency (3). Diameters of approximately greater than 28 mm have empirically been considered as dilated in adult patients (13). With annular stabilization, similar to prosthesis placement, we can anticipate reconfiguration and restriction of the virtual basal ring, so even during diastole, this plane may remain more circular than its native state. In pre-operative planning, therefore, one can assess diastolic area, and calculate an area-derived diameter, as if this plane were circular [Equation I: effective diameter = $2x\sqrt{\left(\frac{area}{\pi}\right)}$] (14). This may provide improved precision in stabilizing the virtual basal ring aiming to achieve valve competency.

Sinuses of valsalva

Though the normal aortic root is often considered

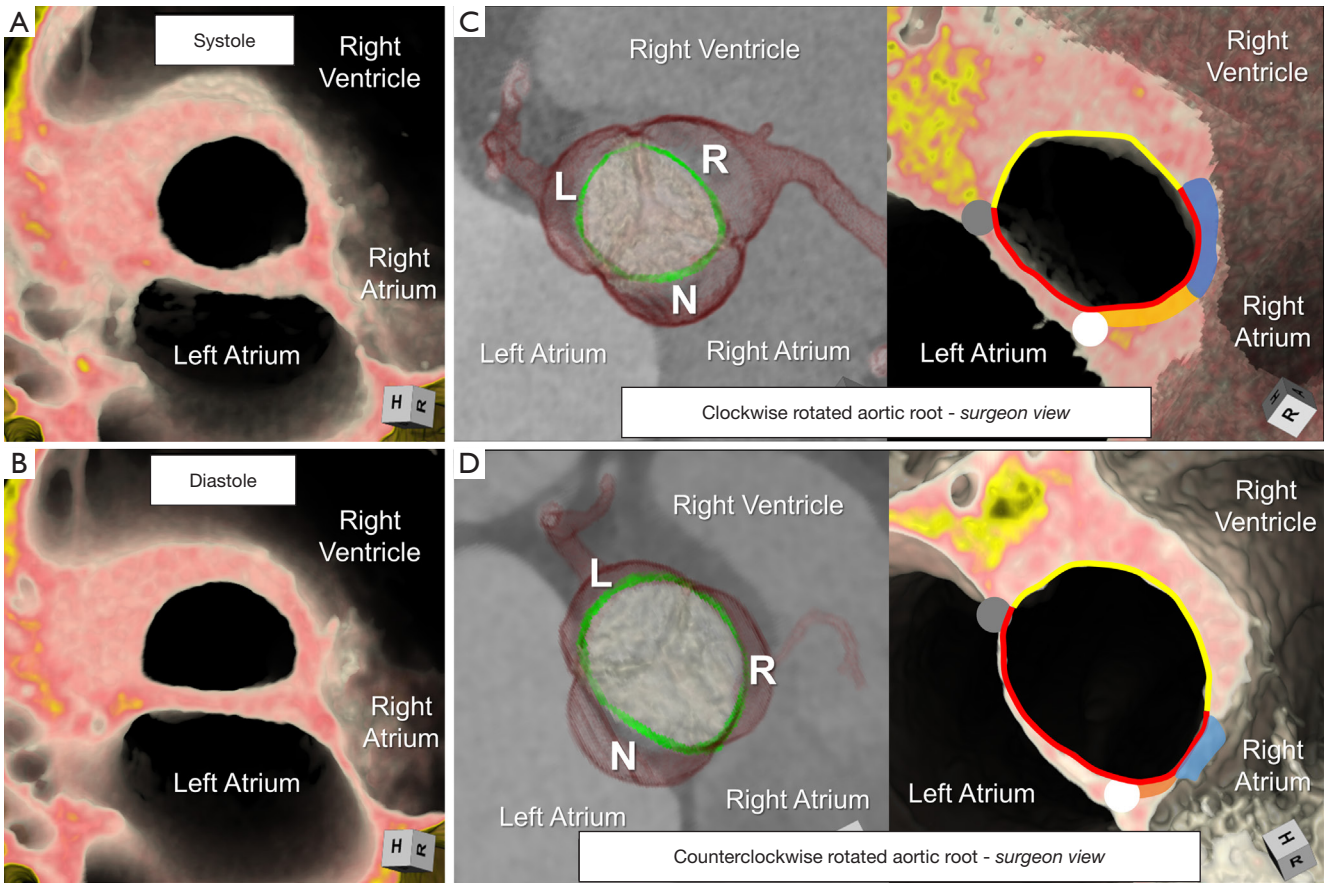

Figure 3 The dynamic virtual basal ring and its variation. (A,B) The dynamic nature of the plane of the virtual basal ring is demonstrated with three-dimensional computed tomographic reconstructions. It is often more circular in systole, becoming elongated and D-shaped in diastole. The rotational position of the aortic root, whether positioned clockwise (C) or counterclockwise (D) relative to the base of the left ventricle will change the orientation of the various sinuses and leaflets to the major and minor dimensions of the plane of the virtual basal ring in diastole (colored green). This has also been demonstrated to correlate with increasing or decreasing fibrous support (red line) of the aortic root, respectively, with corresponding decreasing or increasing muscular support (yellow line). It is important to understand that the conventional description of the rotational position is from the imager view, viewing the root from the apex of the left ventricle. This is the opposite views depicted in (C,D), viewing from the arterial aspect of the valve. The fibrous structures are labeled as in *Figure 2*. L, left coronary sinus; N, non-coronary sinus; R, right coronary sinus.

a relatively symmetrical structure, there are subtle asymmetries of the sinuses worth noting. This is in addition to the obvious asymmetries related to the coronary artery origins. The right and non-coronary sinuses are often larger than the left coronary sinus (2). The interleaflet triangle between these two larger sinuses is often taller, positioning the related commissure higher than the other two (15). This then creates an angle between the plane of the virtual basal ring and sinutubular junction as mentioned later, commonly tilting the aortic root leftward (3).

2D echocardiographic long-axis measurements of the aortic root hover between a center of sinus-to-center of sinus, to off-center, widest sinus-to-sinus, to non-specific center plane. The nadirs of both leaflets may be visualized in the off-center plane, and mark the basal ring. This, however, can only be ascertained with the use of multiplanar reformatting (4,16). The widest sinus-to-sinus measurement will provide, on average, a 3 mm greater difference in sinus dimensions than the center of sinus-to-center of sinus measurement (*Figure 1*) (17).

These challenges are amplified in the significantly asymmetric or congenitally malformed aortic root with important discrepancies reported between standard TTE and CMR (18). It then becomes important in those perceived to have significant interval dilation, or those nearing surgical threshold, to provide a more accurate assessment by cross-sectional, 3D imaging (1,6). Utilizing multiplanar reformatting, three linear methods measured from the short axis of the aortic root have been proposed. Each provides different values in the same patient (*Figure 1*) (4,17). Recent guidelines suggest that the widest dimension reflects the stress seen by the sinus walls (1). Even so, it remains unclear which method may be best. It is clear, however, that utilizing one method over the other will dictate when a patient is perceived to reach surgical thresholds. Of note, a single small study demonstrated that the diastolic measures utilizing the center of sinus-to-center of sinus measurement between the right and non-coronary sinuses by CMR correlated best with the leading edge-to-leading edge measurement by echocardiography (19). In contrast, comparing normative aortic root volumes by CT to these three common short axis linear dimensions, it was the center of sinus-to-opposite commissure measurement that best correlated. This suggests that this method may be the best 2D surrogate of the 3D volume (17). Understanding volumetric values that portend risk towards aortic dissection is a current barrier in applying 3D volumes towards decision-making. Assessment of cross-sectional area indexed to height has been suggested as a potential way forward in both adults and children (1). A value ≥10 cm^2/m has been proposed as a threshold for increased risk of aortic dissection in adults (20,21), with a more recent pediatric and young adult-based study in those with Marfan syndrome suggesting surgical threshold values of 5 to 7 cm^2/m in these younger patients with underlying genetic predisposition (22).

Pending improved understanding of these volumetric and cross-sectional area measurements, standard dimensions continue to be utilized in determining surgical timing. Diameters ≥5.5 cm, or growth ≥0.5 cm/year are generally accepted as surgical thresholds for the general adult population. Smaller values are accepted for those with genetic predisposition, other risk factors, or in established centers of excellence where optimal surgical interventions are consistently achieved (1). For accurate assessment, there should be a low threshold for obtaining some form of cross-sectional imaging, based on institutional availability and expertise. Understanding of which measurement method may be best is not clear. However, what is understood is that there must be institutional consistency and reporting of the measurement method used and timing of the cardiac cycle.

Rotational position of the aortic root

Only recently has the importance of understanding normal variation in the rotational position of the aortic root relative to the base of the left ventricle been elucidated. This variation corresponds with variation in the underlying myocardial versus fibrous support of the aortic root (*Figure 3C,3D*) (10,23), along with variation in the amount of ventricular myocardium incorporated into the bases of the coronary sinuses (11). It is important to note that the standard is to refer to the rotational position as seen by the imager, from the apex of the left ventricle. This is opposite of what is viewed by the surgeon from above. Using the imager view, clockwise rotation refers to when the right coronary sinus is positioned more anteriorly, further away from the right atrium. Counterclockwise rotation refers to when the right coronary sinus is positioned closer to the right atrium (24). The imager can compare the center of the non-coronary sinus to the position of the right fibrous trigone for quantitative assessment (*Figure 4*) (23). Utilizing this quantitative approach in normal adults, a mean angle of approximately +16° with range of −32° to +45° was reported (23). With clockwise rotation, there is a greater proportion of fibrous support, with widening and deepening of the inferoseptal recess, which forms one of the three components of the central fibrous body (*Figures 3C,4B,4D*). In addition, there is a decrease in the myocardium incorporated into the base of the left, and increase in that incorporated into the base of the right coronary sinuses, respectively. The opposite of these collective findings is seen with counterclockwise rotation (*Figures 3D,4C,4E*) (10,11,25).

We are only beginning to understand the implications that corresponding variability in the rotational position and support of the aortic root have on the durability of its valve, the resulting hemodynamics and tissue biomechanics seen by the thoracic aorta, and the relationship between the root and the ventricular components of the conduction axis. Fluid-structure interaction simulations have demonstrated that the extreme of normal clockwise rotational position of the aortic root imparts an increased wall shear stress at the distal aortic root and proximal ascending aorta (26). Clinical studies have confirmed that in both normal adults,

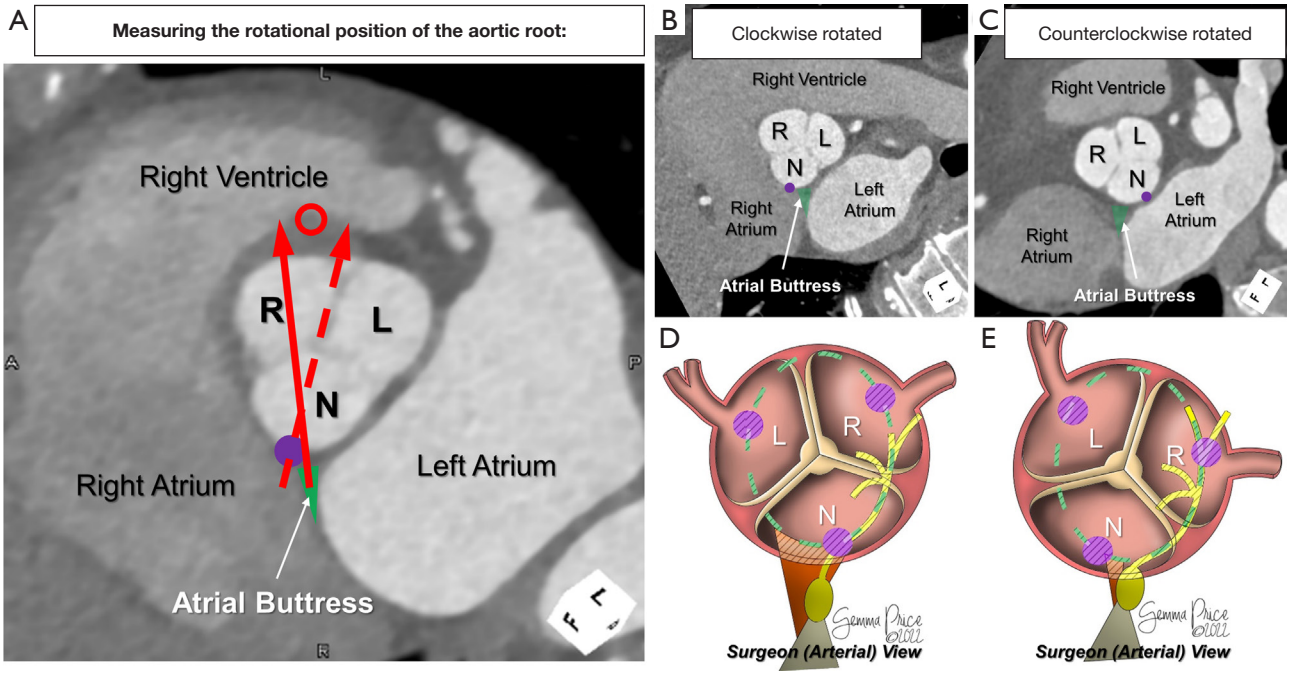

Figure 4 Rotational position of the aortic root. (A) The rotational position of the aortic root is measured from the short axis of the aortic root. A line is placed from the center of the non-coronary sinus (N) (purple circle) to the opposite commissure. A second line is placed along the long axis of the buttress of the atrial septum (green triangle). The angle between (°) represents the rotational position, with a positive value representing clockwise rotation, and a negative value representing counterclockwise rotation. Examples of normal variation in clockwise (B,D) versus counterclockwise (C,E) rotation are demonstrated from an imager/ventricular (viewed by computed tomography) and surgeon/arterial (drawing) view, respectively. (D) Recent investigations have demonstrated that with clockwise rotation, the inferoseptal recess tends to be deep and broad (colored orange). This positions the proximal ventricular components of the conduction axis posterior relative to the circumference below the virtual basal ring (green hashed line). This also tends to position the conduction axis (colored yellow) closer to the non-coronary sinus (N), although relatively inferior to this plane. (E) With counterclockwise rotation, the inferoseptal recess tends to be shallow and narrow, and position the atrioventricular node and proximal ventricular components of the conduction axis closer to the circumference below the plane of the virtual basal ring. In addition, the conduction axis, specifically the left bundle and its superior fascicle, maintains a closer position to the right coronary sinus (R) and plane of the virtual basal ring. The nadirs of leaflet attachment are marked with purple circles. L, left coronary sinus.

and children and young adults with genetic aortopathy syndromes, a clockwise positioned root correlates with progressive dilation of both the aortic root and ascending aorta (27,28). Furthermore, in those with transposition of the great arteries following the arterial switch procedure, the rotational position of the neo-aortic root impacts not only neo-aortic dilation but also neo-aortic valve competency (29).

Building upon our understanding of the conduction system relative to the aortic root, which is further elaborated on later (25,30-32), there is emerging data that the rotational position and its correlation with the central fibrous body may dictate the vulnerability of the conduction axis towards iatrogenic damage. As mentioned, with clockwise rotation there is widening and deepening of the inferoseptal recess. The penetrating bundle will penetrate at the anterior margin of the roof of the inferoseptal recess. The non-branching bundle will then course under the inferior margin of the membranous septum with the left bundle branch originating near the anterior aspect of this inferior margin, and its superior fascicle coursing immediately inferior to the nadir of the right coronary leaflet (25,30,32). In the clockwise positioned root, the proximal ventricular components will then be positioned

outside of the circumference extending below the virtual basal ring plane. The left bundle branch will be relatively more inferior and posteriorly positioned to the nadir of the right coronary leaflet (*Figure 4D*). In the counterclockwise positioned root, the inferoseptal recess becomes narrow and shallow, bringing these proximal components into this circumference, with the left bundle branch commonly extending further anteriorly and in close proximity to the nadir of the right coronary leaflet. These relationships in the counterclockwise positioned root pose increased vulnerability to iatrogenic damage (*Figure 4E*) (32).

Understanding the rotational position has also been suggested to hold implications towards avoiding iatrogenic damage of adjacent structures during valve-sparing aortic root replacement (33). This understanding only scratches the surface of its implications. Variation in the rotational position not only changes the position of the sinuses to adjacent structures, but also towards the orientation of the virtual basal ring plane (*Figure 3C,3D*). Recognition is crucial when evaluating valve competency (3). Most commonly, in the centrally positioned aortic root, the minor axis of the virtual basal ring plane in diastole aligns near the midline of the right coronary leaflet. This is why the right coronary leaflet in the normal aortic root has the smallest measurement of its midline length from nadir to central free edge, or geometric height (15). Variability in rotation changes these relationships, and dilation of the virtual basal ring and sinuses can adversely and asymmetrically impact valve competency related to these subtleties. This understanding further guides surgical personalization as we will elaborate.

Sinutubular junction and ascending aorta

The same concepts regarding limitations of 2D assessment and the additive value of cross-sectional imaging of the previous structures apply to the sinutubular junction and ascending aorta. However, their dimensions are relatively more circular. It becomes important for both the imager and surgeon to recognize that in the normal aortic root, the plane of the sinutubular junction tilts 15°–20° upwards towards the right and non-coronary sinuses relative to that of the virtual basal ring in diastole (2,3). As previously mentioned, this relates to the slightly larger non- and right coronary sinuses and intervening interleaflet triangle when compared to the left coronary sinus and its adjacent interleaflet triangles (2,15). In the congenitally malformed aortic root with fusion between one or more sets of leaflets, the normal semilunar leaflet attachment is perturbed. There is a direct relationship between the degree of leaflet fusion and hypoplasia of the involved interleaflet triangle (Figure S1) (34). Their zenith of attachment will not reach to the normal plane of the sinutubular junction. Determining the plane of the sinutubular junction in the setting of leaflet fusion then becomes more challenging, especially in the presence of effacement of this plane (3).

Dilation and effacement of the sinutubular junction negatively impacts valve competency. Clinical experience, supported by computational modeling studies, suggest that the dimensions of the sinutubular junction should not exceed those of the plane of the virtual basal ring for optimal leaflet coaptation (35). For any patient proceeding towards valve-sparing aortic root replacement, assessment of the sinutubular junction and ascending aorta will determine the need for stabilization of the sinutubular junction, or if a supracoronary ascending aortic support is necessary.

Personalized surgical planning

When surgery is deemed necessary, the consistent high-spatial resolution afforded by CT provides detailed qualitative and quantitative geometrical assessment of the aortic root and its components (3). This information helps determine the repair or replacement strategy, and when thought appropriate, personalize the approach towards valve-sparing aortic root replacement. The ability to provide this information before entering the operating theater has numerous benefits, including the ability for better informed patient counseling. Transesophageal echocardiography (TEE), including 3D imaging with multiplanar reformatting, is then used to solidify this geometric assessment in the pre-operative study (36). This adds fidelity towards the assessment of the components of the leaflets involved in the zones of apposition. The post-operative TEE is then used to assess valve competency and post-repair durability.

Evaluation of the aortic root is simplified when evaluated in terms of its three components: the sinuses, leaflets and interleaflet triangles (2,3). When congenitally malformed, description of its morphology can then be fully implied with description of how the leaflets function and the morphology of the aortic root (Figure S2). For example, the most common form of the bicuspid aortic valve is fully described as a “functionally bileaflet and trisinuate aortic root”. This

Table 1 Cardiac computed tomographic scan acquisition considerations for pre-surgical planning study

Patient characteristics	Computed tomographic scan	Considerations
Severe aortic regurgitation with aneurysmal aortic root dilation +/– aortic stenosis +/– complex repaired or unrepaired congenital heart disease involving the LVOT or aortic root	Retrospective ECG-gated 4D cardiac CT focused on the aortic root	Dose modulation in systole is considered in those with primary regurgitation and no other complex characteristics A subsequent high-pitched spiral acquisition of the chest is considered to evaluate the entirety of the thoracic aorta in those without recent CMR and with known, or concern for significant ascending aortic dilation
Severe aneurysmal aortic root dilation with no more than mild aortic regurgitation	Prospective ECG-gated cardiac CT gated in mid-diastole, or alternatively a high-pitch ECG-triggered spiral acquisition triggered in mid-diastole	–

LVOT, left ventricular outflow tract; ECG, electrocardiogram; 4D, four-dimensional; CT, computed tomography; CMR, cardiac magnetic resonance.

implies that anatomically there are three leaflets, though two are fused together with a corresponding raphe and hypoplastic interleaflet triangle, and that this valve is housed within an aortic root with three sinuses (3,37). In this lesion, description of whether the leaflets are partially or fully fused, and the commissural position, whether symmetrically (160°–180°) or asymmetrically positioned (<160°), may add further value towards surgical decision-making (3,38,39).

Quantitative geometrical assessment of the aortic root and its valve

We have adopted, and improved upon, a geometric approach towards assessment of the aortic root and its components for pre-surgical planning and post-surgical assessment (3,36). This approach is of particular benefit in the incompetent aortic valve, which often coincides with dilation of the virtual basal ring and aortic sinuses, where a valve-sparing operation is pursued (40,41). In both young children and adults reaching surgical thresholds, we obtain a contrasted-enhanced cardiac CT to guide this assessment, optimizing tube settings to minimize radiation exposure. In those with higher heart rates without contraindications, we administer an intravenous beta-blocker to achieve a target heart rate of below 80 beats per minute during scan acquisition. This allows better delineation of the aortic root and its valve. The type of scan acquisition is determined by the patient characteristics, aiming to limit radiation exposure as much as possible (*Table 1*) (3,42).

When four-dimensional data is obtained, for the assessment of valve competency the most quiescent period of the aortic root in mid-diastole is selected. This is often at 70–80% the R-R interval, immediately prior to atrial contraction. Utilizing multiplanar reformatting and marking the plane of the virtual basal ring, a center bisecting plane is achieved to allow accurate assessment of these metrics (*Figure 5*). For comparison, normative values obtained by CT have been established in the adult population (*Table 2*) (15). Such normative values have yet to be established in pediatric patients. Although similar, these CT-based values in adults are slightly different than those achieved *ex vivo* or intraoperatively. This may relate to the latter forms assessing in a non-hemodynamic state with the potential for stretching the leaflets during assessment in the operating theater (15,43,44).

The geometric height and free margin length represent the dimensions of the leaflets (3,15). The geometric height is a curvilinear measurement taken along the midline of the leaflet from its nadir to the center point of its free margin edge (15,43). Values that are less than 80% of normal indicate leaflet retraction. This represents a geometric height approximately less than 16 mm in the normal trileaflet valve, or less than 19 mm in the nonfused leaflet of a functionally bileaflet valve with trisinuate aortic root (44). Attempts at valve-sparing in those with leaflet retraction have demonstrated poorer repair durability when compared to those with leaflet prolapse as the primary mechanism of valve incompetency (45). The free margin length is a curvilinear measure of the distance between the commissures along the edge of the leaflet (3,15). Comparison of these values may help to guide leaflet plication (3). The effective height and coaptation

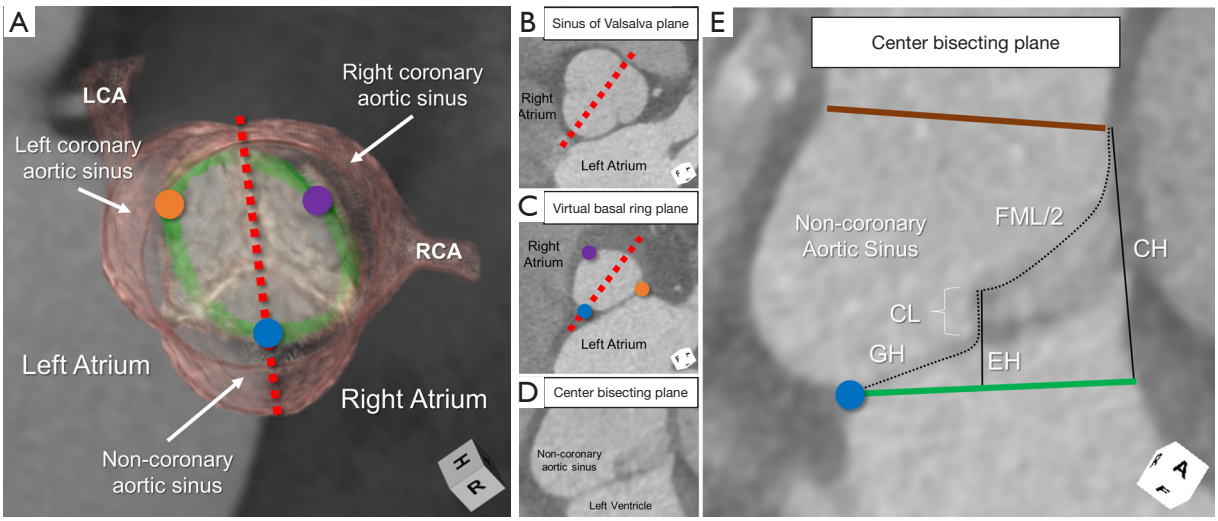

Figure 5 Assessment of the aortic root geometry and measures of leaflet coaptation. (A) A normal aortic root in diastole is demonstrated with a 3D computed tomographic reconstruction. The virtual basal ring is outlined in green, with the nadirs of the left, right and non-coronary leaflets marked with orange, purple and blue circles, respectively. The center bisecting plane through the non-coronary sinus is marked with the red dotted line. The short axis of the aortic root at the sinuses of Valsalva (B) and virtual basal ring (C) are depicted, with the corresponding center bisecting plane. The orthogonal long axis plane is depicted without (D) and with the aortic root metric measurements (E). With multiplanar reformatting, the plane of the virtual basal ring (green line) and sinutubular junction (brown line) can be marked accurately. LCA, left coronary artery; RCA, right coronary artery; CH, commissural height; CL, coaptation length; EH, effective height; FML, free margin length; GH, geometric height; 3D, three-dimensional.

length represent measures of valve coaptation (3). The effective height is the linear measurement from the center of the virtual basal ring to the cephalad edge of the central segment of coaptation of the leaflets. This measure in adults is on average 8–10 mm above the virtual basal ring plane by CT (3,15,46). In the normal valve, the effective height is approximately 45% that of the geometric height (44). Absolute or proportional values less than those stated may indicate leaflet prolapse, requiring central plication. The coaptation length is the linear extent of the segment of apposition involved at the central point of coaptation, at the nodules of Arantius (3). This measure in adults is on average 3–5 mm (15,44). There is a natural increase laterally in the coaptation length between the adjacent lunules of the leaflets (44). However, utilizing the center bisecting plane, one ensures to measure the central point of coaptation for accurate comparison to normative values (3,16). Assessing both the effective height and coaptation length post-operatively utilizing multiplanar reformatting with TEE has been demonstrated to be an important predictor of repair durability. In the adult patient, achieving effective height and coaptation length values of greater than 9 and 5 mm, respectively, has been reported to predict durable repair (47,48). The commissural height is the distance from the virtual basal ring, along the long axis of an interleaflet triangle, to the position of the commissure at the sinutubular junction. In the congenitally malformed aortic root with fusion between leaflets and corresponding hypoplasia of the involved interleaflet triangle, assessment of this metric becomes of increasing importance (*Figure 6*, Figure S1, *Videos S1-S4*) (3,15) In the patient with dilation of the normal trisinuate aortic root, exaggerated differences between the commissural heights may be found related to asymmetric dilation of the sinuses (*Figure 7*).

In the normal aortic root, there are predictable relationships between the dimensions of the various planes within the root with the geometric heights and free margin lengths of the leaflets so as to maintain valve competency. This understanding may be used to guide any valve-sparing strategy (15). Utilizing the Pythagorean theorem, one can roughly estimate the idealized dimension of the virtual basal ring prescribing the desired effective height and coaptation

Table 2 Standardized metrics of the normal aortic root measured in mid-diastole from cardiac computed tomographic scans in a normal Japanese adult population (n=123)

Variable	Value (mm)	Value indexed to BSA (mm/m^2)
Geometric height		
Right coronary aortic leaflet	13.9±1.7	–
Left coronary aortic leaflet	14.7±1.7	–
Non-coronary aortic leaflet	15.3±1.5	–
Mean value	14.7±1.3	8.8±1.1
Free margin length		
Right coronary aortic leaflet	33.9±3.9	–
Left coronary aortic leaflet	31.3±3.6	–
Non-coronary aortic leaflet	32.7±3.8	–
Mean value	32.6±3.6	19.6±2.5
Commissural height (height of the interleaflet triangle)		
Between non-coronary and left coronary aortic sinuses	16.6±2.0	–
Between left and right coronary aortic sinuses	17.4±2.2	–
Between right and non-coronary aortic sinuses	17.9±2.5	–
Mean value	17.3±1.8	10.4±1.3
Effective height	8.6±1.4	5.2±1.1
Coaptation length	3.2±0.8	2.0±0.6

Data derived from study by Izawa *et al.* (15). BSA, body surface area.

length, whether stabilized by a graft or annuloplasty technique, to restore valve competency [Equation II: $(\text{annulus}/2)^2 + (\text{effective height} - \text{coaptation length})^2 = (\text{geometric height} - \text{coaptation length})^2$] (49). This further may be simplified by solely comparing the geometric height and desired effective height (Equation III: geometric height – effective height = annulus/2) (50). These simplistic estimations, however, become increasingly fraught with error in the significantly asymmetric and congenitally malformed root. In addition, these equations do not take into account the thickness of tissues nor the pliability of the aortic wall or leaflets.

Assessment of these metrics illuminate the more common occurrence of an asymmetric mechanism of valve incompetency (*Figure 6*) (3). Insulting features may include asymmetric dilation of the various planes within the aortic root, along with retraction or prolapse of one or more leaflets. In assessing the rotational position of the aortic root, one may then relate the position of the sinuses to the major and minor dimensions of the plane of the virtual basal ring (*Figures 3C,3D,6,7*). This may better help to determine graft sizing. For example, if the midline of a retracted leaflet is parallel with the minor axis of the plane of an oval-shaped virtual basal ring, placing a circular graft that may reduce the major axis, however, may increase the minor axis of this plane, must be taken into account (*Figure 6*). Furthermore, the use of CT in this 3D assessment of the aortic root additionally allows precise evaluation of the position of the coronary arteries, which can vary both in their height and circumferential position within the sinuses (11). This appreciation becomes important not only for the current surgical consideration, but also any subsequent considerations for lifespan planning, which may ultimately include one or more transcatheter valve replacements. Taken together, accurate assessment of the dimensions of the various planes of the aortic root, and

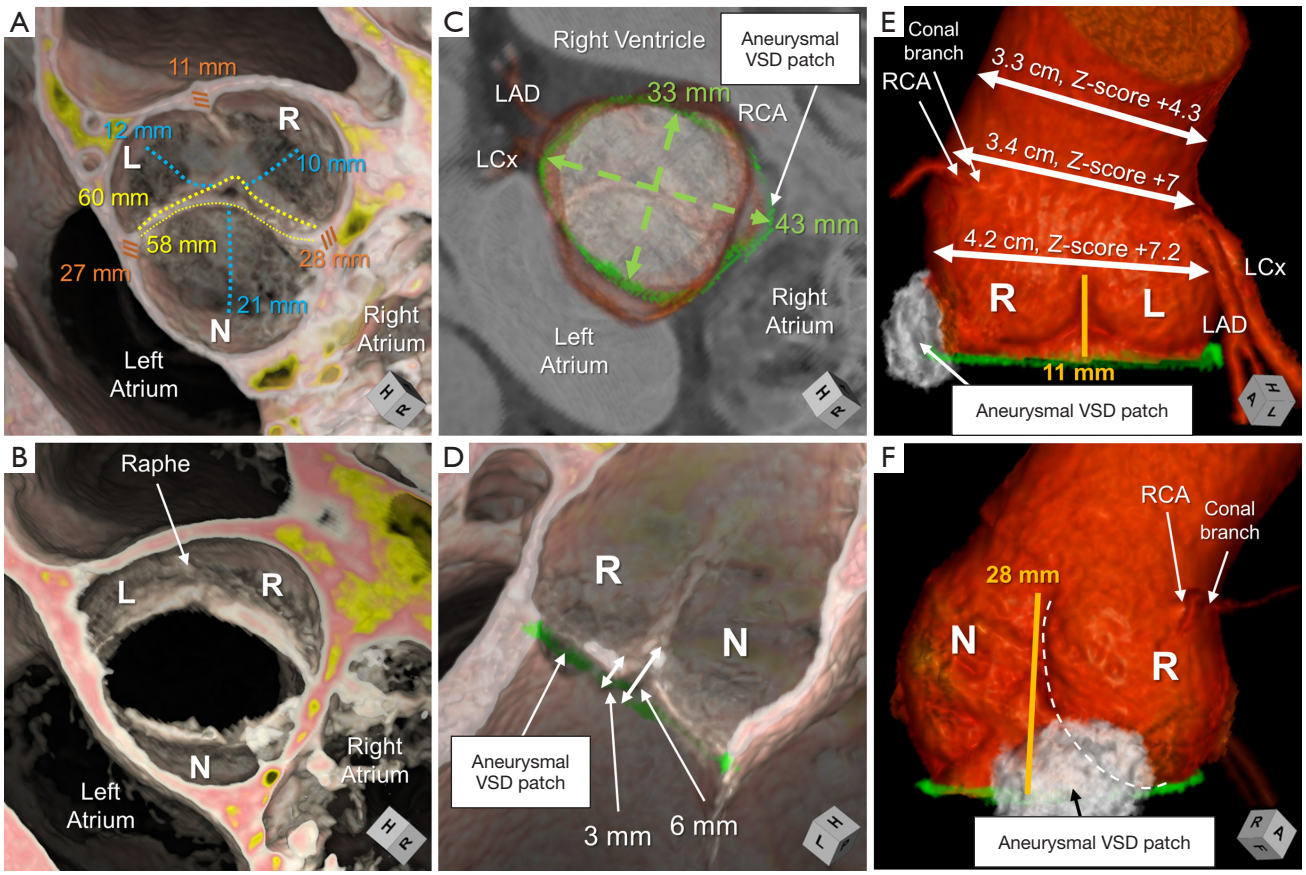

Figure 6 Case example: a retrospective ECG-gated 4D cardiac computed tomographic scan was obtained in an adolescent patient with a functionally bileaflet aortic valve and history of repaired perimembranous VSD, now with severely dilated trisinuate aortic root and severe aortic regurgitation. (A) There is fusion between the coronary leaflets with retracted fused leaflets evident by the geometric heights (10 and 12 mm; geometric heights represented by blue dotted lines) but relatively equal free margin lengths between the fused and unfused leaflets (free margin lengths represented by yellow dotted lines). The commissural height between the fused leaflets is approximately one-third that of the normal commissures (11 *vs.* 27–28 mm; commissural heights represented by orange hashed lines). The two normal commissures are symmetrical, positioned approximately 165 degrees from each other. The coaptation deficiency is visualized centrally, extending to the free edge of the zone of fusion between the coronary leaflets. (B) The valve is depicted in systole, with the prominent raphe visualized over the zone of fusion between the coronary leaflets, and a relatively thickened right coronary leaflet. (C) The virtual basal ring is dilated and eccentric, related to an aneurysmal perimembranous VSD patch. This patch is positioned primarily under the right coronary sinus (R). The minor axis of the virtual basal ring runs parallel to the zone of fusion between the coronary leaflets. (D) The right coronary leaflet is visualized to be thickened and retracted with a low effective height (3 mm) relative to the non-coronary leaflet (6 mm). (E) The aortic root and sinutubular junction are severely dilated with effacement, evident by the Z-scores, with moderate dilation of the ascending aorta. The interleaflet triangle between the fused coronary leaflets is hypoplastic, evident by the commissural height (11 mm). There is separate origin of the LAD and LCx coronary arteries from the left coronary sinus (L), and a separate origin of the conal branch from the right coronary sinus, immediately adjacent to the RCA. (F) The VSD patch is attached superior to the hinge line of the right coronary leaflet (white dashed line), with adjacent fibrous tissue extending onto the right coronary leaflet (appreciated in Panel D). A 30-mm graft was chosen with an internal diameter of approximately 26 mm, which would reduce both the native major and minor axis of the virtual basal ring. The raphe was excised and the free edge of the fused leaflets plicated, maintaining the valve as a functionally bileaflet valve, with the commissures maintained in their symmetrical orientation, accounting for the retracted right coronary leaflet. Fibrous tissue was debrided from the ventricular surface of the right coronary leaflet and the aneurysmal VSD patch tissue was suture plicated. L, left coronary sinus; N, non-coronary sinus; R, right coronary sinus; VSD, ventricular septal defect; LAD, left anterior descending; LCx, left circumflex; RCA, right coronary artery; ECG, electrocardiogram; 4D, four-dimensional.

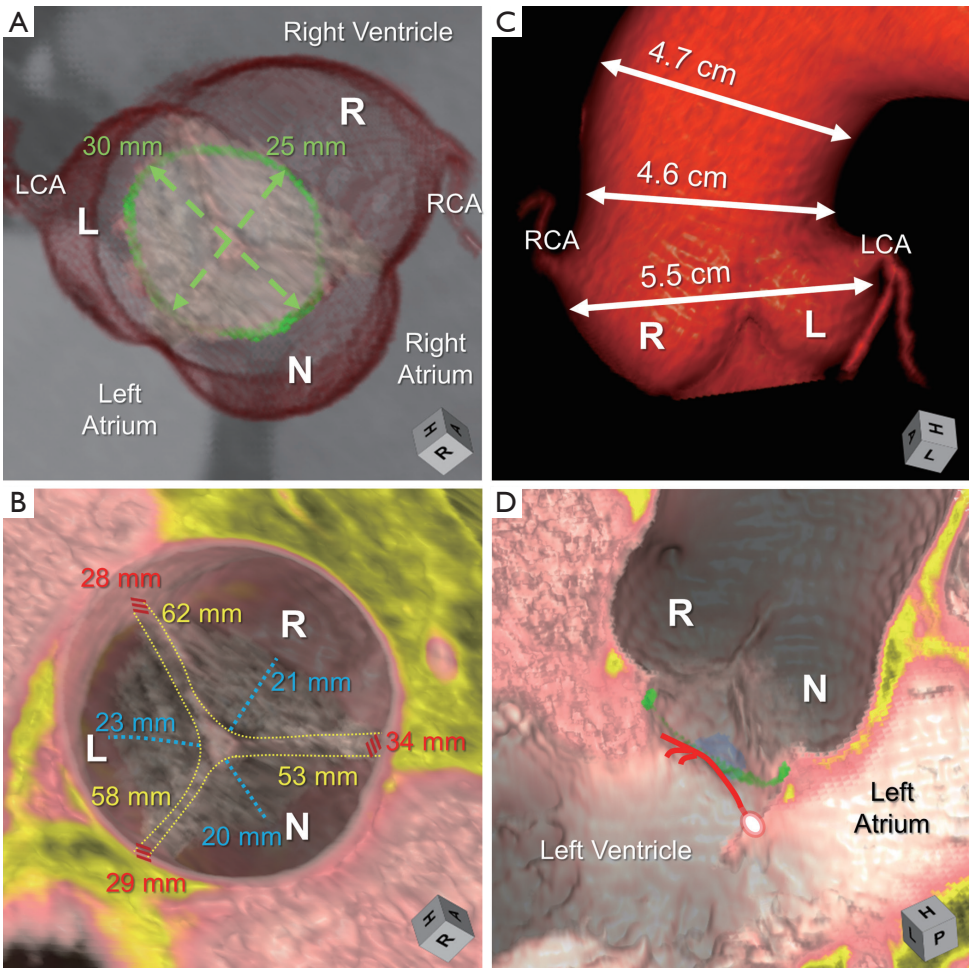

Figure 7 Case example: a prospective ECG-gated cardiac computed tomographic scan was obtained in an adult patient with a normal trileaflet aortic valve with mild regurgitation but severe and asymmetric trisinuate aortic root dilation. (A) Measurements of the aortic dimensions and valve metrics demonstrate asymmetric dilation of the right coronary sinus (R) relative to the other two sinuses. Clockwise rotation of the root positions the minor axis of the virtual basal ring to align with the midline of the right coronary leaflet. (B) This asymmetric dilation results in an exaggerated elongation of the commissural height between the right and non-coronary sinuses (34 mm; commissural heights represented by red hashed lines and red measurement values), with a broader right coronary leaflet represented by the free margin length (62 mm; free margin lengths represented by yellow dotted lines and yellow measurement values). Geometric heights are depicted by the blue dotted lines and blue measurement values. The effective heights and coaptational lengths between the leaflets were normal (not depicted) with no significant coaptation deficiency. (C) The largest dimensions of the proximal thoracic aorta are depicted with severe dilation of the aortic root, dilation and some effacement of the sinutubular junction, and moderate dilation extending into the distal ascending aorta. (D) The anticipated location of the atrioventricular node (white oval with red outline), and subsequent ventricular components of the conduction axis, including the proximal left bundle and its three fascicles are depicted. The latter is estimated to be related to the inferior margin of the membranous septum (colored blue), which courses up to the plane of the virtual basal ring (green line) near the hinge line of the right coronary leaflet. Utilizing this information, a valve-sparing root replacement was pursued. Applying the known geometric heights and desired effective height and coaptation length to the Pythagorean theorem, a 28-mm graft was chosen with an internal diameter of approximately 24 mm, which would reduce both the native major and minor axis of the virtual basal ring. Understanding that the major axis of the virtual basal ring is more or less parallel to the elongated free margin of the right coronary leaflet, central plication of the right coronary leaflet was undertaken, and the commissures where resuspended equidistant around the circumference of the graft. An additional supracoronary ascending aortic graft was placed. L, left coronary sinus; N, non-coronary sinus; R, right coronary sinus; LCA, left coronary artery; RCA, right coronary artery; ECG, electrocardiogram.

Table 3 Recommended approach towards applying this personalized pre-surgical planning approach for aortic valve-sparing operations

Variables	Important values[†]	Surgical considerations
Virtual basal ring	Diameters >26 mm in those with BSA <1.8 m^2, or >28 mm in those with BSA >1.8 m^2 considered dilated in adults	Diastolic configuration is often oval, elliptical or D-shaped Major and minor axis must be related to the orientation of the valve leaflets, and mechanism of valve incompetency • For example, if the midline (or plane of the geometric height) of the leaflet(s) dictating valve incompetency is parallel to the minor axis of the virtual basal ring, a graft size or annuloplasty technique creating an internal diameter larger than the minor axis may be counterproductive Stabilization techniques will confer a more circular shape, even in diastole Pythagorean theorem can be applied to roughly estimate the desired dimension of this plane to restore normal coaptation Equation II: $(annulus/2)^2 + (effective\ height - coaptation\ length)^2 = (geometric\ height - coaptation\ length)^2$
Aortic root rotational position	Normal mean angle =+16° (range, –32° to +45°)	Changes relationship of the aortic root to surrounding structures: • Changes orientation to diastolic configuration of the virtual basal ring plane • Changes orientation to adjacent structures, with implications towards risk of damaging surrounding structures • Implications on implanting the coronary arteries, in particular the right coronary artery • Changes relationship to the ventricular components of the conduction axis
Sinutubular junction	–	Dimensions of the sinutubular junction should not exceed those of the plane of the virtual basal ring for optimal leaflet coaptation
Commissural position	–	In the functionally bileaflet aortic valve with trisinuate aortic root, assessment helps determine whether a functionally bileaflet versus trileaflet repair strategies should be implemented • Symmetric commissures (160°–180°) suggest maintaining the valve as functionally bileaflet, respecting the larger and smaller leaflets created, and adjusting the commissural position accordingly • Very asymmetric commissures (120°–139°) suggest converting the valve to a trileaflet valve
Geometric height	Leaflet retraction: • <16 mm in trileaflet valve • <19 mm in nonfused leaflet of functionally bileaflet valve • Or values <80% of normal	Attempts at valve-sparing in those with leaflet retraction have demonstrated poorer repair durability when compared to those with leaflet prolapse as the primary mechanism of valve incompetency, due to lack of adequate leaflet tissue Graft size should consider how the virtual basal ring plane will be adjusted in the area supporting the retracted leaflet

Table 3 (*continued*)

Table 3 (*continued*)

Variables	Important values[†]	Surgical considerations
Free margin length	Normal mean value =33±4 mm	Comparison of these values may help to guide leaflet plication and commissural repositioning
		In the functionally bileaflet valve, if the valve will be maintained as a functionally bileaflet valve, measuring the free margin of the fused leaflets and comparing to that of the non-fused leaflet will guide need for leaflet plication and commissural repositioning. If the valve will be converted to a trileaflet valve, measuring what the free margin of the two fused leaflets would be once the zone of fusion is divided will help guide resuspension of the leaflets
Commissural height	Normal mean value =17±2 mm	Interleaflet triangle hypoplasia is quantitatively assessed in the functionally bileaflet or unileaflet valve with trisinuate aortic root, and compared to the normal commissural heights. Depending on whether the valve will be maintained/converted to a functionally bileaflet or trileaflet valve, comparison of these values helps to guide leaflet resuspension
Effective height	Normal values >8–10 mm	Absolute values lower than normal suggest leaflet billowing or prolapse, requiring central plication
	Or >45% the geometric height in a normal valve	This measure becomes important to assess with the post-operative TEE to predict durable repair
Coaptation length	Normal values >3–5 mm	In the incompetent valve with central regurgitation, there will be no central coaptation to measure
		This measure becomes important to assess with the post-operative TEE to predict durable repair
Ventricular components of the conduction axis	–	The apex of the inferior pyramidal space can be identified as the approximate location of the atrioventricular node
		The extent of the inferoseptal recess can be interrogated, with its anterior margin abutting the atrioventricular portion of the membranous septum representing the approximate location of the penetrating bundle
		The inferior margin of the membranous septum below the plane of the virtual basal ring can be quantified to understand the proximity the non-branching bundle and origin of the left bundle branch and its superior fascicle will reach near the aortic root, becoming closer anteriorly near the right coronary leaflet. On average, the superior fascicle will be positioned approximately 3 mm inferior to the nadir of the right coronary leaflet (range, 0.4–10.2 mm) (25,32)

[†], important values of the aortic root metrics listed assume proper measurement from a center bisecting plane. BSA, body surface area; TEE, transesophageal echocardiogram.

metrics of leaflet dimensions and coaptation allows for a personalized approach towards aortic valve-sparing surgery (*Table 3*).

Assessment of leaflet substrate and the hemodynamic ventriculo-arterial junction

In addition to the assessment of the dimensions of the aortic root and measurements of the leaflet geometry and valve competency, interrogation of the leaflet substrate is important to determine patient candidacy for any valve-sparing procedure. For proper assessment, the imager and surgeon must fully understand the complexity of the components of the leaflets that form the zones of apposition, and that dictate the integrity of the hemodynamic ventriculo-arterial junction (*Figure 8*).

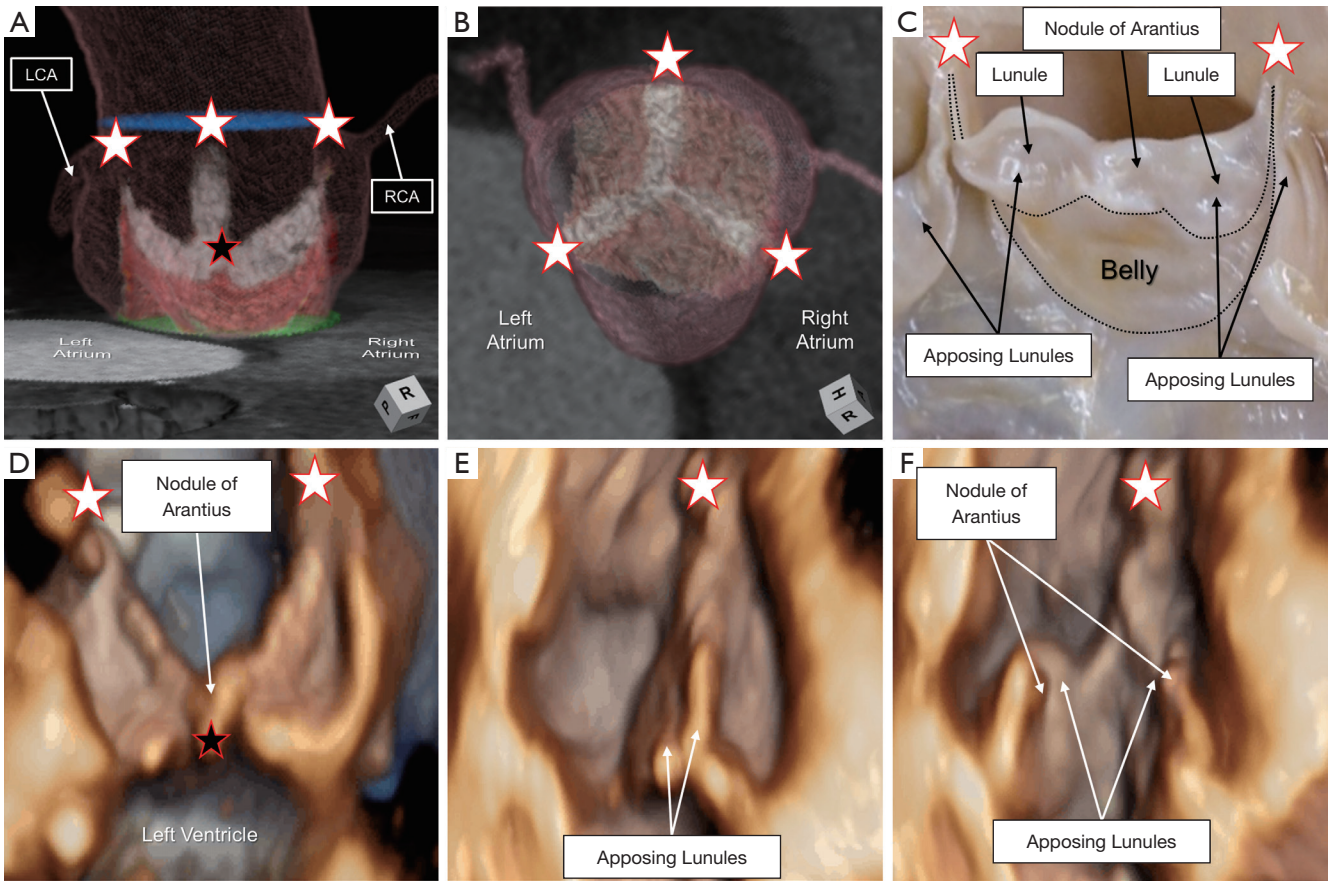

Figure 8 The hemodynamic ventriculo-arterial junction. Three-dimensional computed tomographic reconstruction of the aortic root in diastole viewed in its long (A) and short axis (B) demonstrates the zones of apposition between the three leaflets (colored white). The commissures (white stars with red borders) form the lateral aspect of each zone of apposition, with the zone of apposition formed by apposition of the lunules between each adjacent leaflet, and centrally by the nodule of Arantius of all three leaflets. The belly of each leaflet (colored red) then forms the interface of the hemodynamic ventriculo-arterial junction. The shape of this interface is comprised of three lateral horns spanning from the plane of the virtual basal ring (colored green) to the commissures at the plane of the sinutubular junction (colored blue). In addition, there is a shorter, central horn positioned under the coapting nodules of Arantius (black star with red border in Panel A). (C) The discussed anatomy of the aortic valve leaflet is depicted in the heart specimen. (D) A three-dimensional transesophageal echocardiographic long axis bicommissural view demonstrates the nodules of Arantius coapting centrally with the discussed central horn (black star with red border). Long axis commissural views in diastole (E) and systole (F) demonstrate the components of the leaflets forming the zone of apposition. LCA, left coronary artery; RCA, right coronary artery.

Each aortic valve leaflet is normally attached in semilunar fashion, together creating a crown configuration within the trisinuate aortic root (2). During diastole, the proximal component of the anatomical aortic root is exposed to left ventricular pressures. It is the hemodynamic ventriculo-arterial junction that separates the ventricular versus arterial blood pool during diastole. This junction is formed by the distal components of the leaflets that form the zones of apposition. The zones of apposition represent approximately one-third to one-half of the ventricular surfaces of the aortic valve leaflets (44). The nodules of Arantius are positioned at the center of each leaflet free margin, with all three nodules coapting in the centroid of the root. The coaptation length represents this central coaptation. The effective height minus the coaptation length will represent this central peak above the plane of the virtual basal ring (*Figure 8A,8D*). On either side of the nodule of Arantius are the lunules that extend laterally to each commissure.

The greatest surface area of coaptation is found midway along each lunule. Three larger lateral peaks are then to be found under each commissure. These are measured by the commissural height (*Figure 5E*). The remainder of the ventricular surface of the leaflets, or bellies of the leaflets, extend from their semilunar attachment lines to the inferior aspect of the zones of apposition, bordered peripherally by both commissures. These bellies of the leaflets then serve as the hemodynamic interface in diastole between the blood exposed to ventricular versus arterial pressures (3).

The leaflets can be thickened, calcified or contain other pathology, such as fenestrations, nodularity, perforation, elongation, retraction, bending, prolapse, flail or billowing (3). These pathologies should be evaluated for by any obtained imaging modality, including the importance of direct intraoperative inspection. With the growing experience of transcatheter aortic valve replacement, CT has certainly become the gold standard imaging modality for assessment of leaflet thickening and calcifications (51,52). However, the combination of spatial and temporal resolution afforded by echocardiography, including the benefits of color Doppler interrogation, position it as the main imaging modality for assessing for these subtler leaflet pathologies. Attempt should be made by TTE prior to entering the operating theater. However, given the superior image quality and spatial resolution with less artifact provided by TEE, the pre-operative TEE study obtained prior to surgery or in the operating theater becomes an important component of this assessment (36). This includes both confirmation of the discussed dimensions and metrics utilizing 3D imaging with multiplanar reformatting, and also a more granular assessment of the leaflet substrate and components of the leaflets that dictate the hemodynamic ventriculo-arterial junction.

Measurements of the discussed metrics help in understanding certain pathology, such as leaflet retraction or prolapse, as previously detailed. It is our experience, however, that these more subtle pathologies involving the hemodynamic ventriculo-arterial junction, such as leaflet fenestrations or perforation, often can be missed by standard echocardiographic imaging, CMR and CT (3). Although often considered benign, aortic valve leaflet fenestrations are common, reported to be present in 43% of normal autopsied hearts in a recent pathological study (53). These are commonly located within the lunules of the leaflets, near the commissures. When larger or present in clusters, these fenestrations may negatively impact valve function (53). Utilizing 3D TEE, the imager can thoroughly interrogate the components of the leaflets that comprise the zones of apposition and hemodynamic ventriculo-arterial junction, to further minimize, or hopefully eliminate, any surprises that the surgeon may encounter (*Figure 9*).

Predicting the location of the ventricular components of the conduction axis

The central fibrous body is comprised of the right fibrous trigone, the roof of the inferoseptal recess of the left ventricular outflow tract, and the membranous septum (*Figure 10*) (30,32,54). Whereas the right fibrous trigone is the rightward thickening of the area of fibrous continuity between the anterior leaflet of the mitral valve and the leaflets of the aortic valve, the roof of the inferoseptal recess represents the fibrous tissue between the atrioventricular valves. This latter structure is formed earlier in cardiac development than the right fibrous trigone, insulating the penetrating bundle as it penetrates to reach the crest of the muscular ventricular septum (55). This recess is often bordered by the right fibrous trigone posteriorly, the crest of the muscular ventricular septum inferior and anteriorly, the membranous septum anteriorly, and the non-coronary leaflet of the aortic valve superiorly (30). The inferiorly directed apex of the roof of the inferoseptal recess overlaps with the superiorly directed apex of the inferior pyramidal space, the latter carrying the atrioventricular node (*Figure 10A*) (30,54). It is only recently that we have appreciated the significance of understanding the variability seen in this recess that relates to how the aortic root is transferred to the base of the left ventricle in development, and how it may dictate vulnerability to the ventricular components of the conduction axis (25). This includes the previously discussed variability in the rotational position of the aortic root that correlates with the extent of the inferoseptal recess (*Figure 4D*,*4E*).

The membranous septum also has marked variability in both its position relative to the plane of the virtual basal ring, as well as the angled course of its inferior margin (10,56). Its inferior margin often courses more superiorly as the membranous septum nears the attachment line of the right coronary leaflet (10). This is important, since as early as 1906, Professor Tawara had identified the inferior margin of the membranous septum as the position of the non-branching bundle and origin of the left bundle branch (57). Recent histological investigations have confirmed this anatomy. The left bundle branch and its superior fascicle often continue to ascend the crest of the muscular

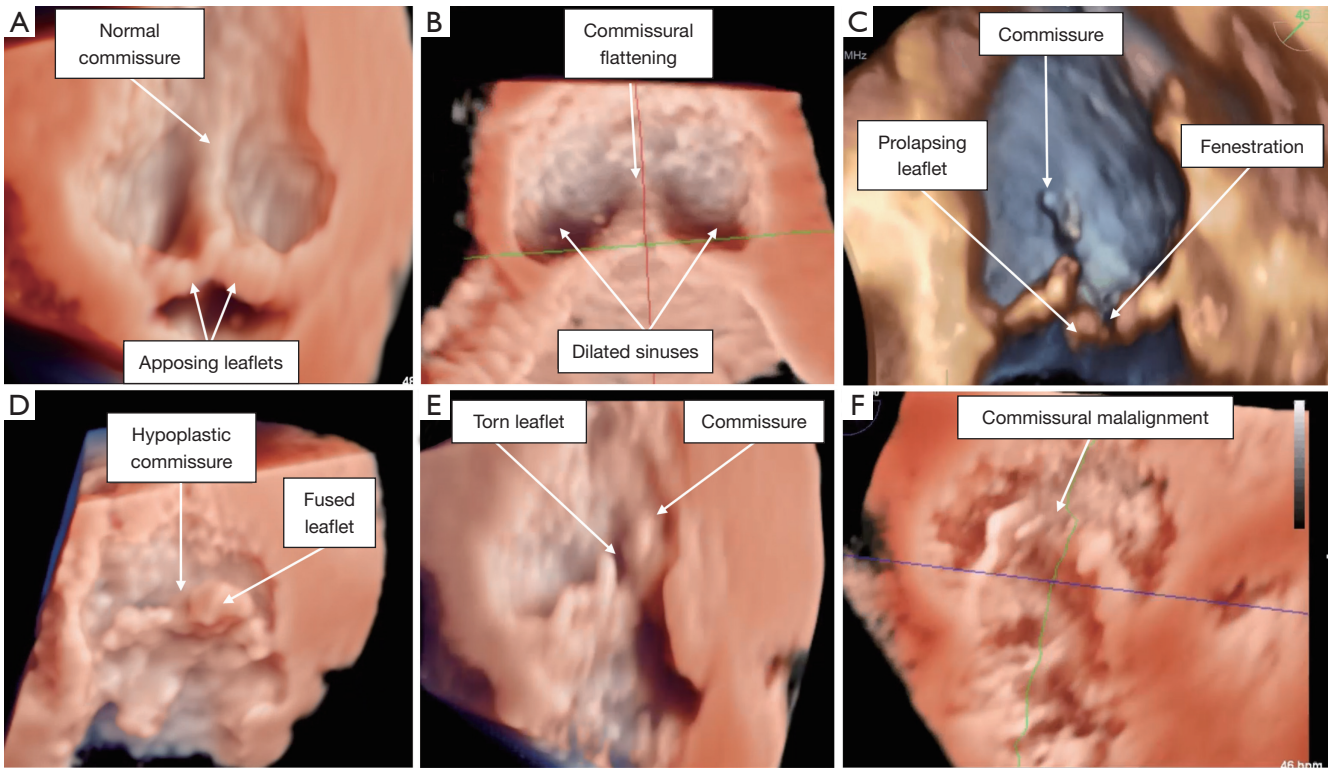

Figure 9 Examples of pathology of the hemodynamic ventriculo-arterial junction. Three-dimensional transesophageal echocardiographic commissural views of the aortic root demonstrate various leaflet pathologies. (A) The aortic valve commissures are seen "en face" from a perpendicular plane from inside the aortic root as demonstrated on this normal trileaflet aortic valve in diastole. (B) The non-left commissural view during diastole of a trileaflet aortic valve demonstrates "leaflet pulling" and commissural flattening due to asymmetric aortic root dilation. Central aortic regurgitation was present. (C) The posterior commissural view during diastole of a functionally bileaflet aortic valve demonstrates prolapse and fenestration of the fused leaflets. Central and eccentric aortic regurgitation was present. (D) The anterior commissural view during systole of a functionally bileaflet aortic valve demonstrates partially fused leaflets and an underdeveloped commissure with hypoplasia of the related interleaflet triangle. (E) The intercoronary commissural view during systole of a trileaflet aortic valve demonstrates a torn left leaflet very close to the commissure. There was commissural, eccentric aortic regurgitation. (F) The posterior commissural view during systole of a functionally bileaflet aortic valve demonstrates commissural malalignment or deficiency between the unfused leaflets. The zenith of leaflet attachment of the fused leaflet is positioned lower than that of the normal leaflet. Central and commissural aortic regurgitation were present.

ventricular septum towards the nadir of the right coronary leaflet, positioned an average distance of only 3 mm inferior to the plane of the virtual basal ring at this location (25,32). This is intuitive in light of the findings that measuring the relationship of the anterior aspect of the inferior margin of the membranous septum to the plane of the virtual basal ring (*Figure 10C*), and comparing to valve implantation depth following transcatheter aortic valve replacement was highly predictive of subsequent conduction damage (31,58).

Utilizing CT assessment, we can accurately delineate the important structures underlying the triangle of Koch and relating to the course of the ventricular components of the conduction axis. Variability in these gross anatomical features correlate with variability seen in the ventricular components of the conduction axis relative to the aortic root (*Figure 10A-10C*) (3,31,32,54). We have recently reported our surgical experience in pediatric and adult patients with both congenital and acquired complex left ventricular outflow tract and thoracic aortic pathology, including an overall incidence of need for pacemaker as 10% (59). This was in keeping with reported values of this higher risk population, with a large multi-center study reporting

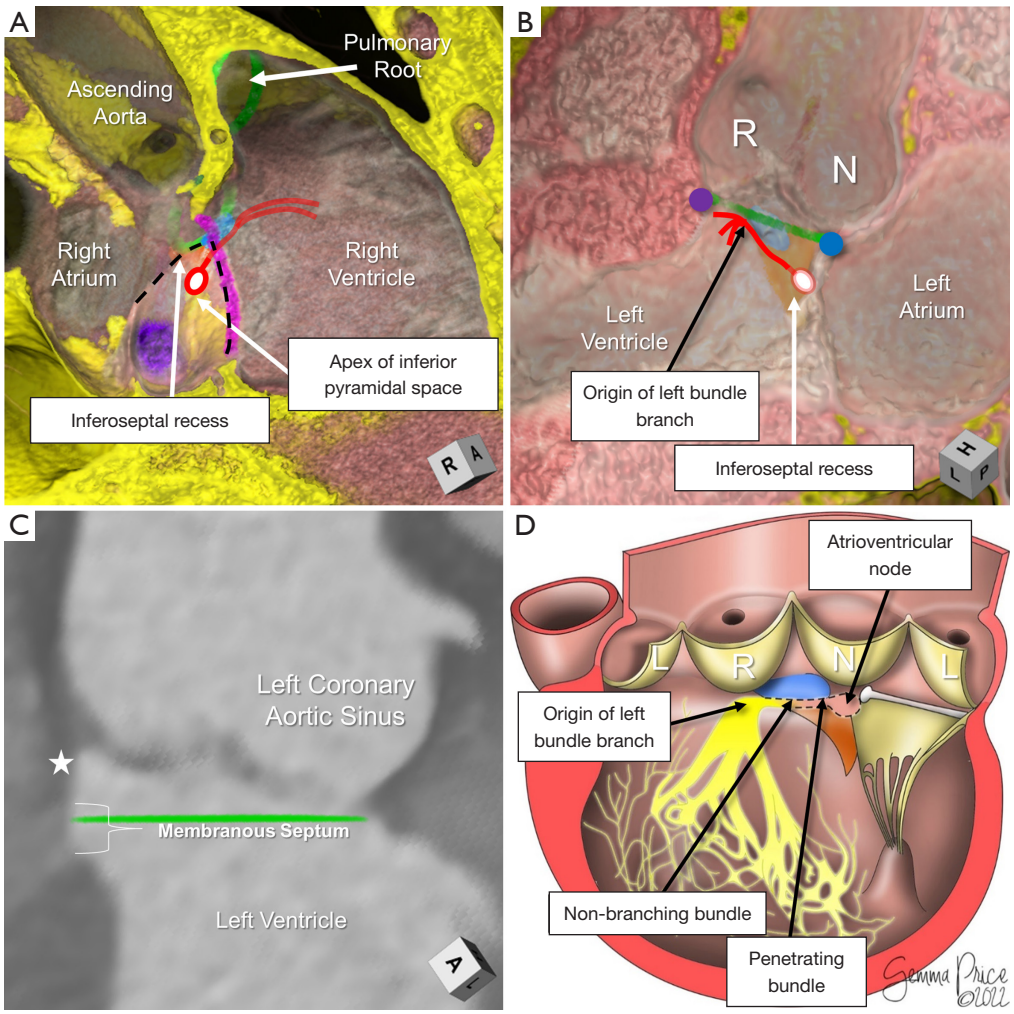

Figure 10 Anatomy of the ventricular components of the conduction axis. Three-dimensional computed tomographic reconstructions viewing the right (A) and left (B) side of the atrial and ventricular septa. (A) The myocardium is made translucent to view the structures behind the triangle of Koch (outlined with black dotted lines, the os of the coronary sinus is colored purple). The triangle points towards the membranous septum (colored blue) that relates to the virtual basal ring of the aortic root (adjacent green circle). The atrioventricular node will be positioned below the apex of the triangle of Koch, at the apex of the inferior pyramidal space. The superiorly directed apex of the inferior pyramidal space will overlap with the downward directed apex of the roof of the inferoseptal recess (colored orange), the latter which is part of the left ventricular outflow tract. The penetrating bundle will penetrate through the junction between the roof of the inferoseptal recess and the posterior aspect of the membranous septum. The non-branching bundle will continue along the inferior margin of the membranous septum, with the left and right bundle branches commonly originating near the anterior aspect of this inferior margin, as depicted with the red lines. (B) The left ventricular outflow tract and aortic root are visualized. The anticipated location of the proximal ventricular components of the conduction axis, including the trifasciculation of the left bundle branch are depicted in red lines. (C) An orthogonal long axis plane to the short axis of the virtual basal ring (colored green) through the height of the membranous septum can be obtained using computed tomographic multiplanar reformatting. This inferior distance from the virtual basal ring to the inferior margin of the membranous septum can be measured at its closest point to anticipate the proximity of the conduction axis to the aortic root (31). Care is taken to differentiate the membranous septum from the superiorly positioned interleaflet triangle and adjacent transverse sinus (white star). (D) Recent investigations support the common adjacency of the left bundle and its superior fascicle to the nadir of the right coronary leaflet as depicted in this illustration (25,32). N, non-coronary sinus; L, left coronary sinus; R, right coronary sinus.

incidences up to 15% depending on the complexity and need for subvalvular manipulation (60). In applying this predictive approach towards our last twenty-four congenital cardiac patients undergoing aortic root and left ventricular outflow tract surgeries, we have had a 0% incidence of need for pacemaker or occurrence of left bundle branch block (59). Although promising in its infancy, this predictive approach requires further validation.

Post-surgical surveillance

The use of multi-modality imaging is instrumental in the post-surgical surveillance of patients following a valve-sparing aortic root replacement. Echocardiography is often adequate to follow valve function, although periodic CMR or CT becomes necessary for evaluation of the entirety of any graft, the remaining native thoracic aorta and the re-implanted coronary arteries. At our institution, we routinely obtain a prospective electrocardiogram (ECG)-gated, contrast-enhanced cardiac CT prior to discharge from their surgical admission. This is to define the post-surgical anatomy, evaluate for dehiscence, pseudoaneurysm, aneurysm or dissection, and to exclude any extracardiac thoracic complications. In the absence of any concerning symptomatology, or concerns raised by routine TTE, the subsequent periodic use of cross-sectional imaging is primarily dictated by the underlying genetic predisposition of the patient, as per suggested guidelines (1).

Conclusions

A personalized approach towards the evaluation of those with aortic root aneurysm, and specifically towards the pre-surgical planning for those considered for aortic valve-sparing operations requires a dynamic, 3D imaging assessment and understanding of the aortic root complex. Such an evaluation is best accomplished using the benefits afforded by multiple imaging modalities. It is our opinion that cardiac CT, with its consistent high spatial resolution, provides additive detailed pre-surgical evaluation of the complex geometry of the aortic root and its structures for personalized aortic valve-sparing operations. In addition, it allows the prediction of the ventricular components of the conduction axis to avoid iatrogenic damage during any related surgical procedure. This allows for appropriate pre-surgical planning and patient counseling, complimented by the additional precision added with TEE and 3D imaging in the operating theater. This preoperative precision evaluation further helps seasoned and less seasoned surgeons to plan and execute the proposed repair accurately.

Acknowledgments

Funding: None.

Footnote

Conflicts of Interest: The authors have no conflicts of interest to declare.

References

1. Writing Committee Members, Isselbacher EM, Preventza O, et al. 2022 ACC/AHA Guideline for the Diagnosis and Management of Aortic Disease: A Report of the American Heart Association/American College of Cardiology Joint Committee on Clinical Practice Guidelines. J Am Coll Cardiol 2022;80:e223-93.
2. Tretter JT, Spicer DE, Mori S, et al. The Significance of the Interleaflet Triangles in Determining the Morphology of Congenitally Abnormal Aortic Valves: Implications for Noninvasive Imaging and Surgical Management. J Am Soc Echocardiogr 2016;29:1131-43.
3. Tretter JT, Izawa Y, Spicer DE, et al. Understanding the Aortic Root Using Computed Tomographic Assessment: A Potential Pathway to Improved Customized Surgical Repair. Circ Cardiovasc Imaging 2021;14:e013134.
4. Tretter JT, Mori S. Two-Dimensional Imaging of a Complex Three-Dimensional Structure: Measurements of Aortic Root Dimensions. J Am Soc Echocardiogr 2019;32:792-4.
5. Hagendorff A, Stoebe S, Tayal B. A systematic approach to 3D echocardiographic assessment of the aortic root. Glob Cardiol Sci Pract 2018;2018:12.
6. Elefteriades JA, Mukherjee SK, Mojibian H. Discrepancies in Measurement of the Thoracic Aorta: JACC Review

Topic of the Week. J Am Coll Cardiol 2020;76:201-17.
7. Greil G, Tandon AA, Silva Vieira M, et al. 3D Whole Heart Imaging for Congenital Heart Disease. Front Pediatr 2017;5:36.
8. Kammerlander AA, Wiesinger M, Duca F, et al. Diagnostic and Prognostic Utility of Cardiac Magnetic Resonance Imaging in Aortic Regurgitation. JACC Cardiovasc Imaging 2019;12:1474-83.
9. De Oliveira Nunes M, Witt DR, Casey SA, et al. Radiation Exposure of Dual-Source Cardiovascular Computed Tomography in Patients With Congenital Heart Disease. JACC Cardiovasc Imaging 2021;14:698-700.
10. Amofa D, Mori S, Toh H, et al. The rotational position of the aortic root related to its underlying ventricular support. Clin Anat 2019;32:1107-17.
11. Toh H, Mori S, Tretter JT, et al. Living Anatomy of the Ventricular Myocardial Crescents Supporting the Coronary Aortic Sinuses. Semin Thorac Cardiovasc Surg 2020;32:230-41.
12. Tretter JT, Spicer DE, Jacobs JP, et al. The aortic valve with two leaflets. JTCVS Open 2022;9:89-90.
13. Federspiel JM, Ehrlich T, Abeln K, et al. Aortic annuloplasty: Subcommissural, intra-annular suture techniques, external and internal rings. JTCVS Tech 2021;7:98-102.
14. Kim WK, Meyer A, Möllmann H, et al. Cyclic changes in area- and perimeter-derived effective dimensions of the aortic annulus measured with multislice computed tomography and comparison with metric intraoperative sizing. Clin Res Cardiol 2016;105:622-9.
15. Izawa Y, Mori S, Tretter JT, et al. Normative Aortic Valvar Measurements in Adults Using Cardiac Computed Tomography - A Potential Guide to Further Sophisticate Aortic Valve-Sparing Surgery. Circ J 2021;85:1059-67.
16. Mori S, Izawa Y, Shimoyama S, et al. Three-Dimensional Understanding of Complexity of the Aortic Root Anatomy as the Basis of Routine Two-Dimensional Echocardiographic Measurements. Circ J 2019;83:2320-3.
17. Suzuki M, Mori S, Izawa Y, et al. Three-dimensional volumetric measurement of the aortic root compared to standard two-dimensional measurements using cardiac computed tomography. Clin Anat 2021;34:333-41.
18. Vis JC, Rodríguez-Palomares JF, Teixidó-Tura G, et al. Implications of Asymmetry and Valvular Morphotype on Echocardiographic Measurements of the Aortic Root in Bicuspid Aortic Valve. J Am Soc Echocardiogr 2019;32:105-12.
19. Rodríguez-Palomares JF, Teixidó-Tura G, Galuppo V, et al. Multimodality Assessment of Ascending Aortic Diameters: Comparison of Different Measurement Methods. J Am Soc Echocardiogr 2016;29:819-826.e4.
20. Masri A, Kalahasti V, Svensson LG, et al. Aortic Cross-Sectional Area/Height Ratio and Outcomes in Patients With a Trileaflet Aortic Valve and a Dilated Aorta. Circulation 2016;134:1724-37.
21. Masri A, Kalahasti V, Svensson LG, et al. Aortic Cross-Sectional Area/Height Ratio and Outcomes in Patients With Bicuspid Aortic Valve and a Dilated Ascending Aorta. Circ Cardiovasc Imaging 2017;10:e006249.
22. Bhimani SA, Rahmy A, Kim S, et al. Optimizing evaluation in pediatric and young adult patients with Marfan syndrome: Novel longitudinal metrics to track growth of aortic structures. J Thorac Cardiovasc Surg 2022;164:724-740.e6.
23. Tretter JT, Mori S, Saremi F, et al. Variations in rotation of the aortic root and membranous septum with implications for transcatheter valve implantation. Heart 2018;104:999-1005.
24. Anderson RH, Spicer DE, Tretter JT. Surgical implications of variations in the anatomy of the aortic root. Eur J Cardiothorac Surg 2022;62:ezac205.
25. Macías Y, Tretter JT, Sánchez-Quintana D, et al. The atrioventricular conduction axis and the aortic root-Inferences for transcatheter replacement of the aortic valve. Clin Anat 2022;35:143-54.
26. Sundström E, Jonnagiri R, Gutmark-Little I, et al. Effects of Normal Variation in the Rotational Position of the Aortic Root on Hemodynamics and Tissue Biomechanics of the Thoracic Aorta. Cardiovasc Eng Technol 2020;11:47-58.
27. Saremi F, Cen S, Tayari N, et al. A correlative study of aortic valve rotation angle and thoracic aortic sizes using ECG gated CT angiography. Eur J Radiol 2017;89:60-6.
28. Powell SK, Almeneisi H, Alsaied T, et al. Rotational Position of the Aortic Root is Associated with Increased Aortic Dimensions in Marfan and Loeys-Dietz Syndrome. Pediatr Cardiol 2021;42:1157-61.
29. Tseng SY, Tretter JT, Gao Z, et al. Aortic root rotational position associates with aortic valvar incompetence and aortic dilation after arterial switch operation for transposition of the great arteries. Int J Cardiovasc Imaging 2023;39:1013-21.
30. Sánchez-Quintana D, Anderson RH, Tretter JT, et al. Anatomy of the conduction tissues 100 years on: what have we learned? Heart 2022;108:1430-7.
31. Tretter JT, Mori S, Anderson RH, et al. Anatomical

predictors of conduction damage after transcatheter implantation of the aortic valve. Open Heart 2019;6:e000972.
32. Tretter JT, Spicer DE, Macías Y, et al. Vulnerability of the ventricular conduction axis during transcatheter aortic valvar implantation: A translational pathologic study. Clin Anat 2023;36:836-46.
33. Oishi K, Arai H, Oi K, et al. The rotational position of the aortic valve: implications for valve-sparing aortic root replacement. Eur J Cardiothorac Surg 2022;62:ezac179.
34. Sundström E, Tretter JT. Impact of variation in interleaflet triangle height between fused leaflets in the functionally bicuspid aortic valve. ASME J of Medical Diagnostics 2022;5:031102.
35. Marom G, Halevi R, Haj-Ali R, et al. Numerical model of the aortic root and valve: optimization of graft size and sinutubular junction to annulus ratio. J Thorac Cardiovasc Surg 2013;146:1227-31.
36. Hagendorff A, Evangelista A, Fehske W, et al. Improvement in the Assessment of Aortic Valve and Aortic Aneurysm Repair by 3-Dimensional Echocardiography. JACC Cardiovasc Imaging 2019;12:2225-44.
37. Anderson RH, Spicer DE, Quintessenza JA, et al. Words and how we use them-Which is to be the master? J Card Surg 2022;37:2481-5.
38. de Kerchove L, Mastrobuoni S, Froede L, et al. Variability of repairable bicuspid aortic valve phenotypes: towards an anatomical and repair-oriented classification. Eur J Cardiothorac Surg 2019;ezz033.
39. Sabet HY, Edwards WD, Tazelaar HD, et al. Congenitally bicuspid aortic valves: a surgical pathology study of 542 cases (1991 through 1996) and a literature review of 2,715 additional cases. Mayo Clin Proc 1999;74:14-26.
40. Schäfers HJ. The 10 Commandments for Aortic Valve Repair. Innovations (Phila) 2019;14:188-98.
41. David T. Reimplantation valve-sparing aortic root replacement is the most durable approach to facilitate aortic valve repair. JTCVS Tech 2021;7:72-8.
42. Tretter JT, Crotty EJ, Lehenbauer DG. 'Form fruste' Aortoventricular Tunnel: Preoperative Computed Tomographic Virtual Dissection Defines This Unusual Variant. Circ Cardiovasc Imaging 2022;15:e014092.
43. Schäfers HJ, Schmied W, Marom G, et al. Cusp height in aortic valves. J Thorac Cardiovasc Surg 2013;146:269-74.
44. De Kerchove L, Momeni M, Aphram G, et al. Free margin length and coaptation surface area in normal tricuspid aortic valve: an anatomical study. Eur J Cardiothorac Surg 2018;53:1040-8.
45. Anand J, Schafstedde M, Giebels C, et al. Significance of Effective Height and Mechanism of Regurgitation in Tricuspid Aortic Valve Repair. Ann Thorac Surg 2023;115:429-35.
46. Schäfers HJ, Bierbach B, Aicher D. A new approach to the assessment of aortic cusp geometry. J Thorac Cardiovasc Surg 2006;132:436-8.
47. Kachroo P, Kelly MO, Bakir NH, et al. Impact of aortic valve effective height following valve-sparing root replacement on postoperative insufficiency and reoperation. J Thorac Cardiovasc Surg 2022;164:1672-1680.e3.
48. Berrebi A, Monin JL, Lansac E. Systematic echocardiographic assessment of aortic regurgitation-what should the surgeon know for aortic valve repair? Ann Cardiothorac Surg 2019;8:331-41.
49. Komiya T, Shimamoto T, Nonaka M, et al. Is small cusp size a limitation for aortic valve repair?†. Eur J Cardiothorac Surg 2019;56:497-502.
50. Tanaka H, Nomura Y, Murakami H, et al. A simplified approach to determine the ventriculoaortic junction diameter in the reimplantation procedures. JTCVS Tech 2022;12:27-31.
51. Cartlidge TR, Bing R, Kwiecinski J, et al. Contrast-enhanced computed tomography assessment of aortic stenosis. Heart 2021;107:1905-11.
52. Khan JM, Rogers T, Waksman R, et al. Hemodynamics and Subclinical Leaflet Thrombosis in Low-Risk Patients Undergoing Transcatheter Aortic Valve Replacement. Circ Cardiovasc Imaging 2019;12:e009608.
53. Dudkiewicz D, Zhingre Sanchez JD, Hołda J, et al. Aortic valve fenestrations: Macroscopic assessment and functional anatomy study. Clin Anat 2023;36:612-7.
54. Tretter JT, Spicer DE, Sánchez-Quintana D, et al. Miniseries 1-Part III: 'Behind the scenes' in the triangle of Koch. Europace 2022;24:455-63.
55. Hikspoors JPJM, Macías Y, Tretter JT, et al. Miniseries 1-Part I: the Development of the atrioventricular conduction axis. Europace 2022;24:432-42.
56. Mori S, Tretter JT, Toba T, et al. Relationship between the membranous septum and the virtual basal ring of the aortic root in candidates for transcatheter implantation of the aortic valve. Clin Anat 2018;31:525-34.
57. Tawara S. Das Reizleitungssystem des Sa¨ugetierherzens. Jena, Germany: Gustav Fischer; 1906.
58. Jørgensen TH, Hansson N, De Backer O, et al. Membranous septum morphology and risk of conduction abnormalities after transcatheter aortic valve implantation.

EuroIntervention 2022;17:1061-9.
59. Tucker DL, Lee LJ, Ahmad M, et al. Surgical strategies to address re-operative complex left ventricular outflow tract and thoracic aortic pathology: Cleveland Clinic children's experience. Cardiol Young 2023. [Epub ahead of print].

Cite this article as: Tretter JT, Burbano-Vera NH, Najm HK. Multi-modality imaging evaluation and pre-surgical planning for aortic valve-sparing operations in patients with aortic root aneurysm. Ann Cardiothorac Surg 2023;12(4):295-317. doi: 10.21037/acs-2023-avs2-0040

doi:10.1017/S1047951122003936.
60. Romer AJ, Tabbutt S, Etheridge SP, et al. Atrioventricular block after congenital heart surgery: Analysis from the Pediatric Cardiac Critical Care Consortium. J Thorac Cardiovasc Surg 2019;157:1168-1177.e2.

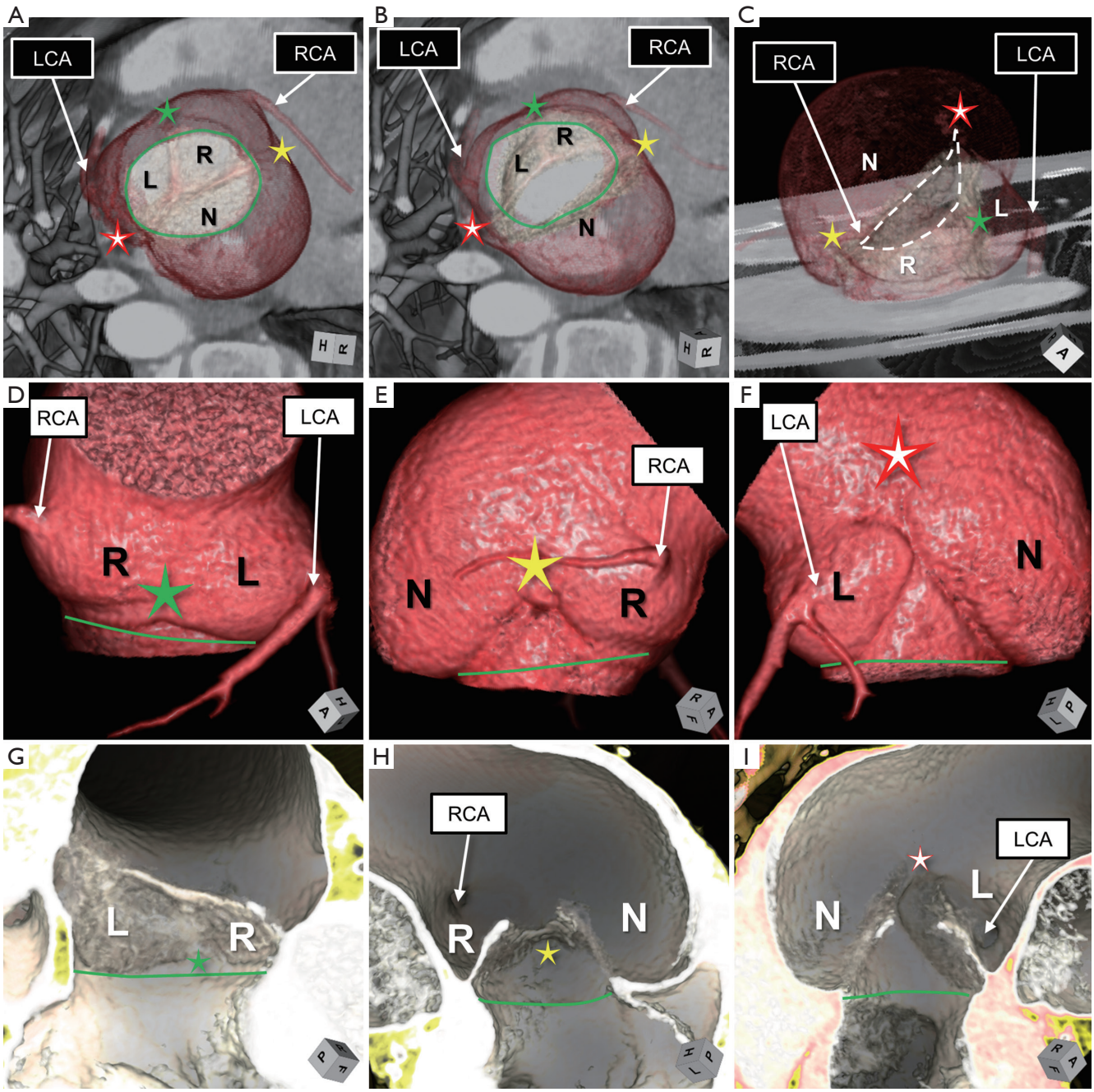

Figure S1 Three-dimensional volume-rendered computed tomographic reconstructions of a functionally unileaflet valve with a trisinuate aortic root are depicted. (A,B) The short axis of the aortic root in diastole (A) and systole (B) are demonstrated. The plane of the virtual basal ring is colored green in all panels. The single commissure is shown by the white star with red borders. The apices of the hypoplastic interleaflet triangles are marked with green and yellow stars. (C) A long axis view highlights the angle of valvular opening (white hashed lines). (D-F) The blood-filled cavity of the aortic root is depicted, with variable degrees of hypoplasia of two of the three interleaflet triangles. (G-I) Corresponding virtual dissections during systole are depicted. L, left coronary leaflet or sinus; N, non-coronary leaflet or sinus; R, right coronary leaflet or sinus; LCA, left coronary artery; RCA, right coronary artery.

https://dx.doi.org/10.21037/acs-2023-avs2-0040

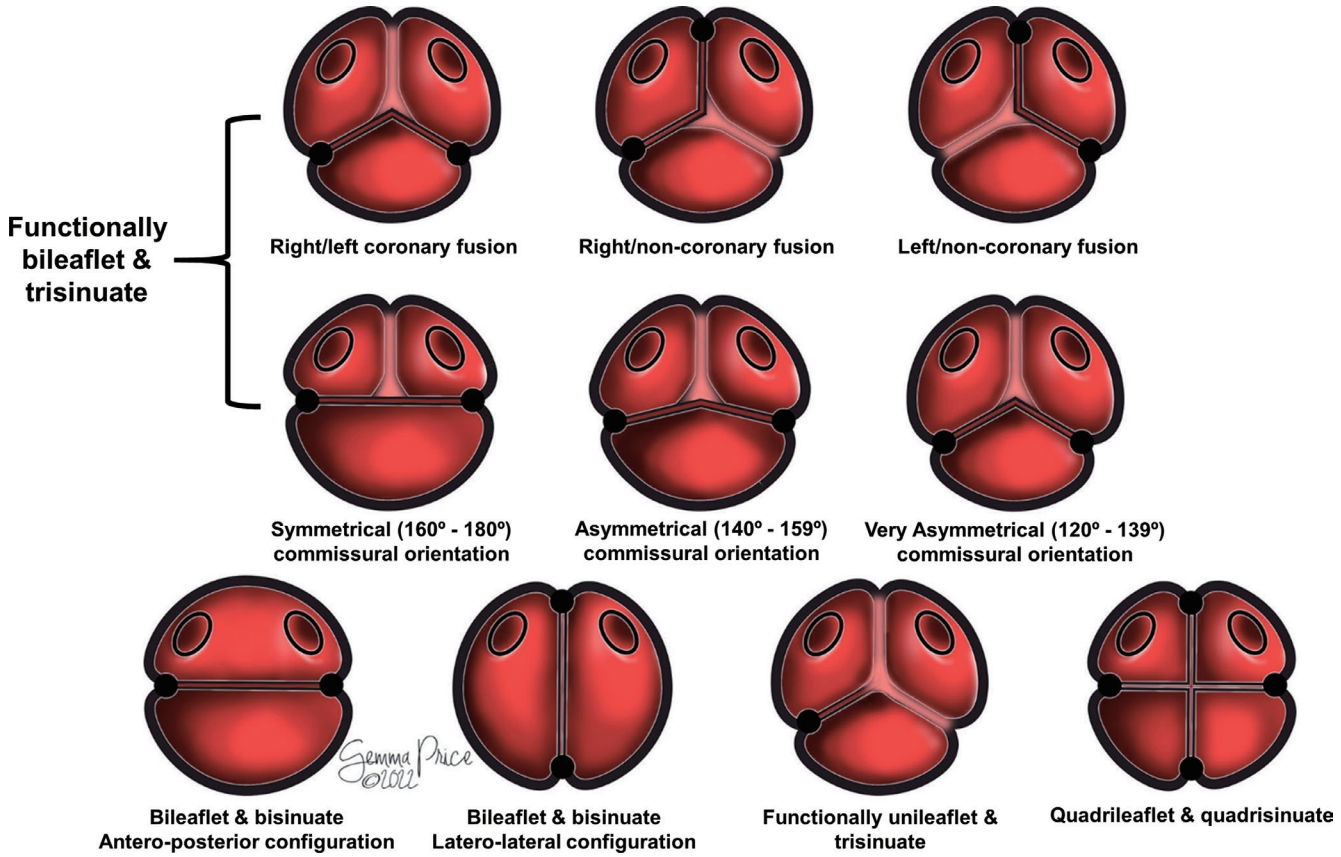

Figure S2 The drawings demonstrate a simplified, yet inclusive classification scheme of the congenitally malformed aortic root recognizing the components of the aortic root, namely the leaflets, sinuses and interleaflet triangles.

https://dx.doi.org/10.21037/acs-2023-avs2-0040